Regime Behavior in the Upper Stratosphere as a Precursor of Stratosphere–Troposphere Coupling in the Northern Winter

HUA LU,[a] LESLEY J. GRAY,[b] PATRICK MARTINEAU,[c] JOHN C. KING,[a] AND THOMAS J. BRACEGIRDLE[a]

[a] *British Antarctic Survey, Cambridge, United Kingdom*
[b] *National Centre for Atmospheric Science, Clarendon Laboratory, Department of Physics, Oxford University, Oxford, United Kingdom*
[c] *Japan Agency for Marine-Earth Science and Technology, Yokosuka, Japan*

(Manuscript received 29 October 2020, in final form 14 May 2021)

ABSTRACT: A new regime index is constructed to capture the seasonal development of the stratospheric polar vortex in the northern winter, based on the standard deviation of Ertel's potential vorticity in the upper stratosphere in November–December. The narrow-jet flow regime is characterized by a polar vortex that is more confined to high latitudes in the early winter upper stratosphere. This upper-level vortex configuration is more susceptible to the disturbances of upward propagating planetary-scale Rossby waves; the stratospheric polar vortex thus weakens earlier and is vertically shallower. The wide-jet flow regime is characterized by a broader-than-average polar vortex that extends further into the subtropics in the early winter upper stratosphere. The polar night jet then gradually strengthens, moves poleward, and penetrates deep into the lowermost stratosphere, with a sharply defined polar vortex edge due to more frequent Rossby wave breaking. Composite difference analyses show that the wide- and narrow-jet regimes, defined in the uppermost stratosphere in November–December, lead to different circulation anomalies of the lower stratosphere and the troposphere in January–February, offering the potential for improved predictability of subseasonal to seasonal forecasts up to two months ahead. The lower-tropospheric responses in January–February are zonally asymmetric. The narrow-jet regime projects most strongly over the North Atlantic, with an equatorward-shifted and/or broader midlatitude westerly jet. The wide-jet-regime response is characterized by a weakened midlatitude westerly jet over the North Pacific. The two flow regimes also differ in their impacts on the storm track over western Europe and the east coast of North America, which may have implications for extreme weather events in those regions.

KEYWORDS: Arctic Oscillation; Planetary waves; Potential vorticity; Rossby waves; Stratospheric circulation; Wave breaking; North Atlantic Oscillation; Pacific-North American pattern/oscillation; Stratosphere-troposphere coupling; Troposphere; Winter/cool season

1. Introduction

A large body of literature has shown that the winter stratosphere influences tropospheric circulation in the Northern Hemisphere (NH; e.g., Baldwin and Dunkerton 2001; Gerber et al. 2009; Kidston et al. 2015). The influence primarily projects onto the North Atlantic Oscillation (NAO), which in turn is associated with shifts in the position and strength of storm tracks, thereby affecting regional weather and climate (e.g., Scaife et al. 2005; Charlton-Perez et al. 2018). Extensive research has studied coupling between the stratosphere and the troposphere in association with major stratospheric sudden warmings (SSWs; Mitchell et al. 2013; Sigmond et al. 2013; Maycock et al. 2020), polar-night jet oscillations (PJO; Kuroda and Kodera 2004; Hitchcock and Shepherd 2013), downward wave coupling (Perlwitz and Harnik 2003), lower-stratospheric control (Scott and Polvani 2004; Martineau et al. 2018), the role of tropospheric eddies (Simpson et al. 2009), and tropospheric precursors to SSWs (White et al. 2018). However, exploiting knowledge of these vertical connections to improve predictability at subseasonal to seasonal time scales has had limited success (Domeisen et al. 2020).

Dynamical coupling between the stratosphere and the troposphere during northern winter has often been investigated based on the northern annular mode (NAM) (Thompson and Wallace 1998, 2000; Baldwin and Dunkerton 2001; Gerber et al. 2009; Kidston et al. 2015). In the stratosphere, the NAM characterizes variations in the strength of the polar vortex, with a positive NAM indicating a stronger-than-average vortex. In the troposphere, the NAM is also called the Arctic Oscillation (AO), which primarily characterizes meridional shifts in the extratropical westerly jets, with a positive AO indicating a poleward shift (Thompson and Wallace 1998). The NAM (and the tropospheric AO) is primarily associated with the geopotential height over the polar cap (Baldwin and Thompson 2009). Anomalies in the stratospheric NAM tend to precede the tropospheric AO anomalies and the propagation from 10 hPa to the surface takes ~15 days on average (Christiansen 2001), suggesting predictive implications for tropospheric weather on a week-to-month time scale given the state of the stratospheric polar cap (Baldwin and Dunkerton 2001; Baldwin and Thompson 2009). While climate models with a better-resolved stratosphere indeed exhibit the improved seasonal forecasts of near-surface weather (Kidston et al. 2015; Scaife et al. 2005, 2016), questions remain over whether the stratosphere only influences the troposphere through this zonally symmetric mode of variability or whether the influence is in fact regime dependent in the sense that zonal asymmetry or variability outside of the polar cap may also be important (Domeisen et al. 2020).

In this context, one region that has received less attention is the winter upper stratosphere (7–1 hPa, 35–50 km). The northern winter upper stratosphere is highly variable, due to perturbations

Corresponding author: Hua Lu, hlu@bas.ac.uk

DOI: 10.1175/JCLI-D-20-0831.1

by planetary-scale Rossby waves (PRWs), gravity wave breaking and/or instability of the polar night jet (PNJ; Gray et al. 2003; Kuroda and Kodera 2004; Greer et al. 2013; Albers and Birner 2014). Both quasi-stationary PRWs and traveling anticyclones are present at these altitudes (Harvey et al. 2002). They disturb the polar vortex via eddy transport, wave breaking, and wave–wave interactions (O'Neill and Pope 1988; O'Neill et al. 1994; Greer et al. 2015). Extreme stratospheric events such as SSWs are both preceded and followed by upper-stratospheric anomalies (Manney et al. 2008; Greer et al. 2013, 2015). Several model-based studies find that the timing and frequency of SSWs are highly sensitive to background flow conditions as well as wave–wave interactions in the upper stratosphere, highlighting the fact that the region is not a passive recipient of wave forcing from below (Gray et al. 2003, 2020; Lindgren and Sheshadri 2020). These studies indicate that anomalies in the upper stratosphere, a layer containing only ~0.2% of the total air of the atmosphere, can alter the columnwise, vertically propagating PRWs and influence the circulation deep into the troposphere. Using a stratosphere–mesosphere coupled model, Gray et al. (2003) showed a sensitivity of stratospheric flow regimes to the subtropical upper stratosphere. They found that imposing very strong (weak) wave forcing at the lower boundary of their model resulted in a weaker (stronger) polar vortex, as expected. However, for wave forcing of intermediate magnitude, a parameter space was found within which the stratospheric response was no longer linearly dependent on the strength of the lower boundary wave forcing. Instead, the polar vortex evolution depended critically on the upper-level variability. They highlighted the role of anticyclones that propagate eastward and quasi-horizontally from low to high latitudes, where they interact with the polar vortex. The upper-level variability was found to significantly influence the vertical Eliassen–Palm (EP) fluxes at the lower boundary of the model. Using the same model, O'Neill and Pope (1988) showed that nonlinear wave–wave interaction in the upper stratosphere leads to localized, rapid growth of disturbances as well as lower-level barotropic responses. Similarly, Hitchcock and Haynes (2016) imposed SSW-like, easterly zonal-mean anomalies in the extratropical upper stratosphere at ~2 hPa in an idealized troposphere–stratosphere coupled model and found an equatorward shift of the midlatitude westerly jet in the troposphere a few of weeks later.

A range of different flow regimes have been identified in the northern winter stratosphere in previous research (Gray et al. 2003; Kodera et al. 2003). For example, using *k*-means clustering, Coughlin and Gray (2009) found two well-separated states in the winter stratosphere with 10% of the days in a warm disturbed state associated with SSWs and 90% of the days in a cold undisturbed state. The two states are best distinguished based on the zonal-mean zonal winds in the polar upper stratosphere. The upper stratosphere has also been shown to exhibit strong regime behavior during the recovery phase of SSWs, with only a subset of SSWs followed by the prolonged descent of zonal-mean anomalies while shallow, short-lived anomalies were featured after the others (Hitchcock and Shepherd 2013; Kodera et al. 2016). The early winter upper stratosphere can be either in a radiatively driven, nonlinear inviscid regime or a dynamically driven, quasigeostrophic regime, depending on the amplitude of wave disturbances (Tung 1986; Kodera and Kuroda 2002). Midwinter evolution of the stratospheric polar vortex is sensitive to early winter background conditions in the equatorial upper stratosphere and lower mesosphere (Kodera et al. 2003; Gray et al. 2003, 2020). An anomalously cold, undisturbed midwinter vortex is often preceded by an anomalously strong westerly jet in the subtropical upper stratosphere/lower mesosphere in early winter (Kodera and Kuroda 2002; Gray 2003; Kodera et al. 2003). However, although polar vortex influences and evolution have been examined extensively, there has been relatively little research on how the early winter state of the upper stratosphere influences vertical coupling both within the stratosphere and with the underlying troposphere. Also, the polar vortex starts to develop in the upper stratosphere, where the flow is highly zonally asymmetric (Harvey et al. 2002; Manney et al. 2008) and the jet structure in early winter upper stratosphere could play a crucial role in subsequent wave propagation and breaking (Polvani and Saravanan 2000). A better understanding and representation of the connection between the early winter upper stratosphere and the lower parts of the atmosphere is likely to improve predictability at the subseasonal to seasonal time scales.

Our goal here is to provide a new index that facilitates an early winter geometric identification of the structure of the stratospheric polar vortex that leads to different development of the stratosphere–troposphere system later in the winter. In particular, we aim to take into account the fact that circulation in the upper stratosphere is zonally asymmetric as traveling anticyclones frequently embedded in the flow interact with the planetary-scale quasi-stationary anticyclones (O'Neill and Pope 1988; Harvey et al. 2002; Greer et al. 2013, 2015). We characterize this zonal asymmetry using empirical orthogonal functions (EOFs) of the standard deviation of the Ertel's potential vorticity (EPV) fields at 1500 K (~42 km). Based on the leading EOF mode of the November–December (ND) EPV fields, an early winter flow regime index is constructed that separates the northern winter into two distinct flow regimes. Composite analyses are then performed for a range of circulation variables in both the stratosphere and the troposphere and show that the state of the early winter upper stratosphere characterized in this way influences the subsequent development of the stratospheric polar vortex. The early winter upper-stratospheric flow regimes are also found to influence the troposphere in mid-to-late winter (i.e., January–February). The tropospheric responses are detected in the vicinity of the Atlantic and Pacific westerly jets. The flow regimes are found to also influence the midlatitude storm track, especially over western Europe.

The paper is organized as follows: In section 2 we describe the reanalysis data and diagnostics used. In section 3, we first provide details on how the regime index is constructed (section 3a). We then perform composite analyses to show how the stratospheric polar vortex evolves with time and differs between the two flow regimes (section 3b). We then move on to examine longitudinal and vertical variations in December when the two flow regimes differ most in the stratosphere (section 3c). Results of tropospheric responses are then

presented in section 3d. In section 3e we examine the extent to which the new regime index is related to the more commonly used NAM index, including how the two indices are correlated, and how the new regime index compares with the NAM in terms of predictability and persistence. We then investigate possible mechanisms by studying the upper-stratospheric waveguide in early winter and the role of Rossby wave breaking (RWB; section 3f). Finally, in section 4, we present our conclusions with a discussion of how the new regime index may contribute to improved subseasonal to seasonal forecasts.

2. Data and methods

a. Reanalysis datasets

The reanalysis datasets used here are the Climate Forecast System Reanalysis (CFSR) of the National Centers for Environmental Prediction (NCEP) for the period of 1979–2010 and its extension from the Climate Forecast System, version 2 (CFSv2), that covers the period 2011–17 (Saha et al. 2010, 2014). Jointly, they cover the 1979–2017 period (39 years in total). (The data were obtained from https://cfs.ncep.noaa.gov/cfsr/).

Both datasets were generated by NCEP's CFS, which assimilated satellite observations, ground-based observations, and radiosondes. Observed carbon dioxide, aerosols, other trace gases, and solar variations were also included. By using a coupled atmosphere–ocean forecast model, both CFSR and CFSv2 incorporated the interactions among atmosphere, land, ocean, and sea ice. The model's vertical resolution is ~1 km below 10 hPa and increases to 3–5 km in the upper stratosphere. To date, they are the only reanalysis products that provide isentropic-level data higher than 850 K (~10 hPa). This is the key reason this reanalysis product is chosen. CFSR and CFSv2 data are used at a 2.5° horizontal grid spacing on 16 potential temperature levels from 270 to 1500 K (equivalent to around 900–2 hPa or 1–45 km). The results presented below are not sensitive to possible jumps induced by a switch over from CFSR to CFSv2 as similar results are obtained if data from CFSv2 are excluded (not shown). A subset of the diagnostics has also been applied to other reanalysis datasets including ERA-Interim, JRA-55, and MERRA-2 at and below 850 K. Qualitatively similar results are obtained (not shown).

b. Diagnostics

EPV, denoted P herein, is a dynamical quantity that provides insight into PRW propagation and breaking (McIntyre and Palmer 1983). It is also best suited for capturing the dynamical edge of the stratospheric polar vortex and variability around it (Harvey et al. 2002). To capture the variability around the westerly jet in the early winter upper stratosphere, standard deviations of the daily mean EPV, during November–December, σ_P hereafter, are first estimated at each grid point north of the equator at 1500 K (~42 km) for each winter. Data from the entire NH are included because the westerly jet often spirals from the equator to the Arctic. The EOFs of σ_P are determined from the longitude–latitude matrix of November–December standard deviation of daily EPV for the period 1979–2017, following the procedure described by Baldwin et al. (2009), in which the data matrix is first weighted by $\sqrt{\cos\phi}$ to compensate for the reduced atmospheric mass at higher latitudes. The resulting spatial maps of the EOFs are then divided by $\sqrt{\cos\phi}$ and a new regime index is then constructed based on the leading EOF as described in section 3a. Composite analyses of a range of circulation variables are performed to study regime behavior in terms of seasonal development of the stratospheric polar vortex and its subsequent impact on the troposphere in mid-to-late winter. The statistical significance of the composite differences is estimated using two-tailed Student's t test. When the p value is smaller than 0.05, the difference is regarded as statistically significant and referred to as a signal in the text.

The stratospheric waveguide is identified by the distribution of meridional gradient of zonal-mean EPV ($\overline{P}_\phi$) since PRWs can only propagate in regions where $\overline{P}_\phi > 0$. Wave absorption associated with EPV mixing across the polar vortex edge is normally accompanied by a reduction of $\overline{P}_\phi$ and mean zonal winds $\overline{u}$ near the polar vortex edge. RWB, identified by reversals in meridional PV gradient, instead reshapes the polar vortex by moving its edge gradually toward the pole (McIntyre and Palmer 1983). Hitchman and Huesmann (2007) further found that the relationship among RWB frequency, PV reversal strength, and PV gradient is complex and varies geographically. While steep $\overline{P}_\phi$ at the vortex edge increases the resilience of the vortex edge to wave breaking whereby it imposes a dynamical constraint on the latitudinal extent of wave breaking, waves with a large enough amplitude can overcome a given PV gradient and the waves in the regions with strong meridional temperature gradients tend to break. In the latter case, the strength of RWB is linearly related to daily variability but not to $\overline{P}_\phi$. These two types of wave–mean flow interactions tend to coexist in the NH winter stratosphere; their relative importance and seasonal development can nevertheless lead to significant differences in the polar vortex structure and seasonal development (Waugh and Dritschel 1999; Polvani and Saravanan 2000).

We do not attempt to provide a synoptic account of individual RWB events. Instead, our aim is to assess the relative importance of RWB in affecting the latitude–height structure and seasonal evolution of the stratospheric polar vortex following different early winter upper-stratospheric conditions. RWB frequency is examined here by counting the number of days when $P_\phi < 0$ at each grid point over a month or season and the zonal-average of this gridpoint metric represents a statistical measure of RWB (Hitchman and Huesmann 2007). This diagnostic is denoted by $\overline{\gamma}$ hereafter. The term $\overline{\gamma}$ has previously been used to study the modulation of the polar vortex by the quasi-biennial oscillation (QBO; Hitchman and Huesmann 2009; White et al. 2015). Lu et al. (2020) recently showed that the cumulative effect of RWB in the upper stratosphere during the westerly phase of the QBO plays a major role in the observed late winter reversal of the Holton–Tan effect (Holton and Tan 1980; Lu et al. 2008).

Disturbances in the upper stratosphere involve both quasi-stationary PRWs and high-frequency, synoptic-scale traveling anticyclones (Harvey et al. 2002; Gray et al. 2003, 2013, 2015). Breaking of traveling anticyclones and small-scale waves can result in zonally asymmetric, high-frequency variation in the background waveguide. This effect is measured here by

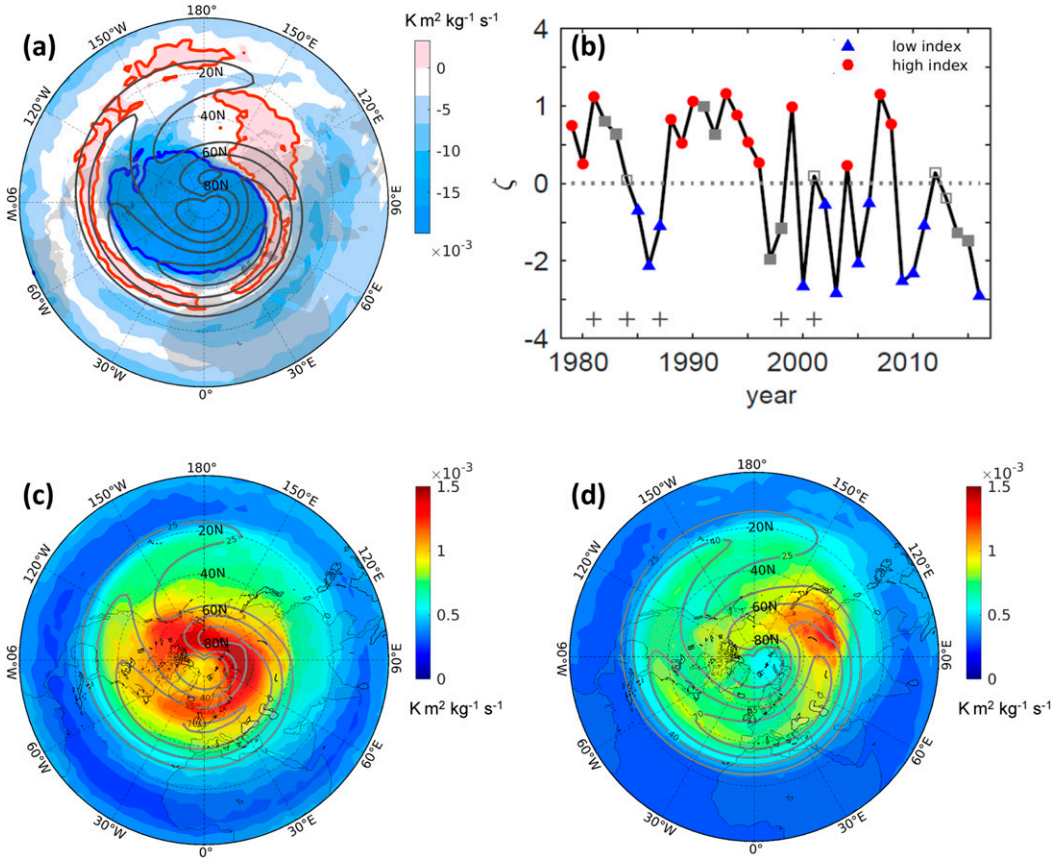

FIG. 1. (a) EOF1 of the standard deviation of daily EPV at 1500 K during November–December. The blue and red contours indicate 50% percentiles of the negative and positive values of the EOF1. Climatological zonal winds are shown as gray contours (25–70 m s^{-1} with an interval of 15 m s^{-1}). (b) Time series of the regime index ζ. Blue triangles (red circles) indicate the low (and high) index composite. Solid gray squares are those affected by the major volcanic eruptions and major ENSO. Empty gray squares are winters having too small ζ. Pluses indicate winters with a December major SSW. (c) November–December-averaged standard deviation of daily EPV (K m^2 kg^{-1} s^{-1}; shaded) and zonal winds (m s^{-1}; gray contours) for the low-index composite. (d) As in (c), but for the high-index composite.

$$\vartheta = \text{std}\left[\sqrt{(P'_\lambda)^2 + (P'_\phi)^2}\right], \tag{1}$$

where P'_λ and P'_ϕ are 9-day high-pass filtered zonal and meridional EPV derivatives. Localized regions with large values of ϑ signify in situ wave generation and nonlinear wave interactions (O'Neill and Pope 1988; Sivan et al. 2016). According to Lindgren and Sheshadri (2020), persistently large wave–wave interactions in the upper stratosphere can lead to up to 37% reduction of SSW frequency, and thus on average a more stable midwinter polar vortex.

3. Results

a. Definition of the flow regimes

In this section, a flow regime index is constructed based on the standard deviation of daily EPV at 1500 K (~2 hPa or 42 km) in early winter.

Figure 1a shows the leading EOF (EOF1) of the November–December standard deviation of daily EPV σ_P at 1500 K. Climatological mean November–December zonal winds of 1979–2017 are contoured to provide dynamical context. This EOF1 accounts for 40% of interannual variability in σ_P for the NH, with the second and third modes only accounting for 9% and 6%, respectively (not shown). The solid red and blue contours indicate 50th percentiles of the positive and negative values of the EOF1, which are equal to 0.0021 and −0.012 K m^2 kg^{-1} s^{-1}, respectively.

EOF1 is characterized by large negative (blue) values poleward of 60°N and intermediate negative values at 15°–40°N over the North Atlantic and Eurasia. Positive (red) values are found along a narrow latitude band on the equatorward flank of the westerly jet that swirls eastward from the subtropical North Pacific into the Arctic over Chukchi Sea. A region of positive values is also evident in the region 30°–60°N, 120°–150°E near the jet exit upstream from the Aleutian high (AH), which is a large-scale, quasi-stationary anticyclone that is climatologically centered over the North Pacific near the date line. EOF1 has relatively small values in the region of the AH itself, consistent with the quasi-stationary nature of the AH

TABLE 1. Winters in the low-index ($\zeta < 0$, i.e., narrow jet) and high-index ($\zeta > 0$, i.e., wide jet) composites. Those affected by major volcanic eruptions, major ENSO, and with nearly zero value of ζ, i.e., $|\zeta| < 0.25$ are also listed. Winters with $^{+}$ had a major SSW in early winter, all of which were in December (Butler et al. 2015). Winters with $^{\#}$ had a major SSW in late winter, i.e., January–March.

$\zeta < 0$		$\zeta > 0$		Volcano	ENSO	$\lvert\zeta\rvert < 0.25$
1985/86$^{\#}$	1986/87$^{\#}$	1979/80$^{\#}$	1980/81$^{\#}$	1982/83	1997/98	1984/85$^{+\#}$
1987/88$^{+\#}$	2000/01$^{\#}$	1981/82^{+}	1988/89$^{\#}$	1983/84$^{\#}$	1998/99$^{+\#}$	2001/02^{+}
2002/03$^{\#}$	2003/04$^{\#}$	1989/90	1990/91	1991/92	2014/15	2012/13$^{\#}$
2005/06$^{\#}$	2006/07$^{\#}$	1993/94	1994/95	1992/93	2015/16	2013/14
2009/10$^{\#}$	2010/11	1995/96	1996/97			
2011/12	2016/17	1999/2000$^{\#}$	2004/05			
		2007/08$^{\#}$	2008/09$^{\#}$			

(Harvey and Hitchman 1996). On the other hand, on relatively short time scales (days to weeks), the amplitude and structure of the AH varies rapidly with noticeable east–west shifts, which has been linked to traveling anticyclones (Harvey and Hitchman 1996). However, the extent to which this short time scale, transient AH variability is influenced by or interacts with the two upper-stratospheric flow regimes cannot be properly examined with the diagnostics used in this paper. This question is therefore left for future research.

Since the maximum polar vortex winds often extend well into the subtropics (as shown from the climatological winds) the EOF in Fig. 1a was derived using data from the full hemisphere. The main features highlighted by the EOF are the negative region centered roughly over the pole (inside the vortex) and the positive region on the equatorward side of the maxima in vortex winds. Despite its relatively small amplitude, we find that the variability on the equatorward flank of the westerly jet, which is not captured by the commonly used NAM index, plays an important role in providing additional extended predictability in the lower stratosphere and the troposphere in mid-to-late winter. To better capture such variability, we choose a regime index ζ based on the differences

$$\zeta = \widetilde{\mathrm{EOF1}}_{p50} - \widetilde{\mathrm{EOF1}}_{n50}, \tag{2}$$

where $\widetilde{\mathrm{EOF1}}_{p50}$ ($\widetilde{\mathrm{EOF1}}_{n50}$) is the normalized areal average of the upper (lower) 50th percentile of positive (negative) values of the EOF1. The regime index ζ effectively captures the seesaw pattern between the two main features that exhibit the largest EPV variability. All results were additionally tested using the first principal component (PC1) to select the two regimes instead of ζ. They were found to be qualitatively similar, since the two indices are highly correlated ($r = 0.85$). However, the magnitude of the PC1 is excessively controlled by the variability within the polar cap, downplaying the variability on the equatorward flank of the westerly jet. In addition, careful inspection reveals that a few winters had relatively large PC1 values because of variability from the low latitudes, away from the main vortex-related features. For these reasons, the percentile-based Eq. (2) was chosen to define the flow regimes.

Figure 1b shows the time series of the regime index ζ. The low- and high-index winters are indicated by blue triangles and red dots. To avoid contamination from the abnormal radiative effects of volcanic aerosols and disturbances induced by major ENSO events, we excluded those winters that were affected by those events defined by monthly ENSO-3.4 time series (gray filled squares). We also exclude the winters having close to zero value of ζ, that is, $|\zeta| < 0.25$, (gray empty squares). A list of the winters in each category can be found in Table 1.

Note that the regime index ζ and the associated low- and high-index composites are defined solely based on EPV at 1500 K (near 2 hPa, ~42 km) in early winter (November–December). The regimes are not biased by the occurrence of an SSW in early winter since both flow regimes include one major SSW each in December (years with a major SSW in early winter are indicated in Fig. 1b by a plus sign, also see Table 1). Also, the regime index ζ is not highly correlated with the QBO at 50 hPa ($r = 0.1$, $p = 0.5$) and neither the low-index nor the high-index composite show any clear bias toward either phase of the QBO. Hence, the differences between the two flow regimes examined hereafter are not due to the presence or otherwise of an early winter SSW and they cannot be interpreted as a manifestation of the Holton–Tan effect (Holton and Tan 1980).

It is evident from Fig. 1b that more (less) winters before (after) 2000 have a positive (negative) value of ζ, with 11 versus 3 winters belonging to the positive phase but 3 versus 9 belonging to the negative phase. Thus, there is a multidecadal variation in the upper-stratospheric flow regimes. The wide-jet regime broadly coincides with winters that were observed to be less disturbed in the 1990s while the narrow-jet regime coincides with more disturbed winters in the 2000s (Domeisen 2019). Noticeable exceptions are the winters of 2007/08 and 2008/09; both are in the wide-jet regime but were extremely disturbed, with major SSWs occurring in middle winter (Butler et al. 2015).

Figures 1c and 1d show the November–December standard deviation σ_P at 1500 K for the low- and the high-index composite, respectively. The low-index composite is dominated by σ_P values that peak on the poleward flank of the polar night jet (Fig. 1c). Large values of σ_P on the poleward flank of the PNJ in the upper stratosphere have previously been linked to unstable PRWs induced by barotropic/baroclinic instability (Greer et al. 2013, 2015). In contrast, the high-index composite is dominated by large values of σ_P in a localized region near the jet exit at 90°–150°E, 35°–60°N (Fig. 1d). Also, the polar vortex jet is broader

and extends farther equatorward in the high-index composite than the low-index composite (see also Figs. 2 and 3). This is most evident at 25°–45°N, 30°W–120°E where u is stronger in the high-index composite and over the Chukchi Sea at 150°E–150°W, 60°–80°N where u is stronger in the low-index composite (indicated by the gray contours in Figs. 1c,d). For simplicity and to facilitate our discussions based on a physically meaningful terminology, the low-index composite is referred to as the narrow-jet regime, while the high-index composite is referred to the wide-jet regime hereafter.

b. Seasonal evolution

In this section, we present evidence to show that seasonal development of the stratospheric polar vortex is affected by the early winter flow regimes in the upper stratosphere.

Figure 2 shows the latitude–height cross sections of monthly averaged composites of zonal-mean zonal wind $\overline{u}$ for the narrow-jet (Figs. 2a–e) and wide-jet (Figs. 2f–j) regimes and the corresponding differences (Figs. 2k–o) from November to March. October is excluded because no significant differences can be detected in that month.

For a given winter month, the early winter upper-stratospheric flow regimes show distinct differences in both the shape and strength of the polar vortex. In the narrow-jet regime (Figs. 2a–e), a strong polar vortex is found in November and December (Figs. 2a,b) but it becomes substantially weakened from January onward (Figs. 2c–e). Also, the meridional gradient of zonal wind $\overline{u}_\phi$ is relatively weak in the climatological surfzone between 20° and 40°N, and the axis of maximum $\overline{u}$ remains fixed in latitude at 55°–65°N throughout the winter. In contrast, the polar vortex in the wide-jet regime is noticeably wider in the upper stratosphere during November and December (Figs. 2f,g). From January onward, the polar vortex continues to strengthen and shifts poleward (Figs. 2h–j) so that the maximum winds migrate from around 40°N in November to 65°N in February. This is accompanied by a marked deceleration of zonal winds in the surfzone at 20°–40°N, thus tightened $\overline{u}_\phi$ at the polar vortex edge. The PNJ also penetrates deeper into the lowermost stratosphere around January/February (Figs. 2h,i).

The differences between the wide-jet and the narrow-jet regimes in the stratosphere are marked by enhanced westerlies in the subtropical upper stratosphere that migrate poleward and downward from November to February, accompanied by easterly differences in the surfzone at 20°–40°N in January–February (Figs. 2k–o). In March, the differences between these two flow regimes become small in magnitude and statistically insignificant (Fig. 2o). In summary, these comparisons highlight a generally weaker and more disturbed polar vortex in mid-to-late winter in the narrow-jet regime and a stronger, deeper, and more poleward-shifted polar vortex in the wide-jet winters. Using satellite data, Dunkerton and Delisi (1986) found similar poleward and downward movements of the polar vortex in the 1979/80 winter (which belongs to the wide-jet regime). By analyzing the daily PV evolution, they suggested that RWB played an essential role in the polar vortex development and acted to precondition the SSW.

Wind differences are also found in the upper troposphere (noting that the regime selection is based solely on the upper-stratospheric flow). Westerly differences appear first in November at 60°–70°N, indicating a stronger, poleward-shifted tropospheric jet (by $\sim 3\,\mathrm{m\,s^{-1}}$) in the wide-jet regime (Fig. 2k). Easterly differences ($\sim 4\,\mathrm{m\,s^{-1}}$) then emerge on the poleward flank of the subtropical jet at 30°–40°N, 350–450 K during December, indicating a weaker tropospheric subtropical jet in the wide-jet regime (Fig. 2l). The pair of westerly and easterly $\overline{u}$ differences merge with those from the upper stratosphere in January and the effect persists through to February (Figs. 2m,n).

The early winter jet characteristics of the two flow regimes are quantitatively summarized in Figs. 3a and 3b, which shows the latitudinal profiles of monthly zonal-mean zonal winds $\overline{u}$ at the upper-stratospheric level used to define the regimes (1500 K) in November and December, together with their 95% confidence intervals and one-standard deviations. In November, $\overline{u}$ peaks at 55°–60°N with a mean value of $49\,\mathrm{m\,s^{-1}}$ for the narrow-jet composite but at 35°–40°N with a mean value of $45\,\mathrm{m\,s^{-1}}$ for the wide-jet composite. In December, the differences are accentuated. The narrow-jet composite $\overline{u}$ peaks at 55°–65°N with a mean value of $46\,\mathrm{m\,s^{-1}}$ but at 35°–45°N with a mean value of $61\,\mathrm{m\,s^{-1}}$ for the wide-jet composite. Also, $\overline{u}$ is noticeably more variable for the narrow-jet regime, especially near 60°–70°N, consistent with the more disturbed nature of the PNJ shown in Figs. 2a–2e and 1c.

The composite difference is largest at 25°–45°N, where the narrow- and wide-jet composite $\overline{u}$ are well separated by more than one standard deviation in both months. Figure 3c puts the composite differences at 25°–45°N in the context of all winters. It shows a scatterplot between the regime index ζ and zonal-mean zonal wind $\overline{u}$, area-averaged over the latitude band of 25°–45°N at 1500 K in December. The zonal-mean zonal wind $\overline{u}$ is positively correlated with the flow index ζ with $r = 0.61$ ($p < 0.01$). The average wind speed in this region is $51\,\mathrm{m\,s^{-1}}$ for the wide-jet regime but is only $25\,\mathrm{m\,s^{-1}}$ for the narrow-jet regime and the difference ($26\,\mathrm{m\,s^{-1}}$) amounts to nearly 60% of the climatological $\overline{u}$ at 25°–45°N, 1500 K in December. We also note that the winters excluded from the two composites are randomly scattered with ζ varying from -2 to 2.

c. Vertical and longitudinal structure

Figure 4 shows composite differences in zonal wind u (Figs. 4a–d) and temperature T (Figs. 4e–h) at four isentropic levels from the uppermost (1500 K) to the lowermost stratosphere (450 K) in December when the regime development starts to emerge in the middle to lower stratosphere. Climatological December mean zonal winds are gray-contoured for reference. As expected, the largest differences in u are in the upper stratosphere at 1500 K (Fig. 4a), with positive differences ($>40\,\mathrm{m\,s^{-1}}$) on the equatorward flank of the westerly jet at 25°–45°N (generally referred to as the "vortex edge") while easterly differences ($\sim 10\,\mathrm{m\,s^{-1}}$) straddle at high latitudes (in the "vortex core") and in the subtropics (i.e., the "extra vortex" region) (Harvey et al. 2002; Manney et al. 2008). Similar zonal wind differences are found at lower levels except that the signal becomes progressively weaker and confined to the North Pacific sector (Figs. 4c,d) and the wind differences tilt westward with height. Such behavior is similar

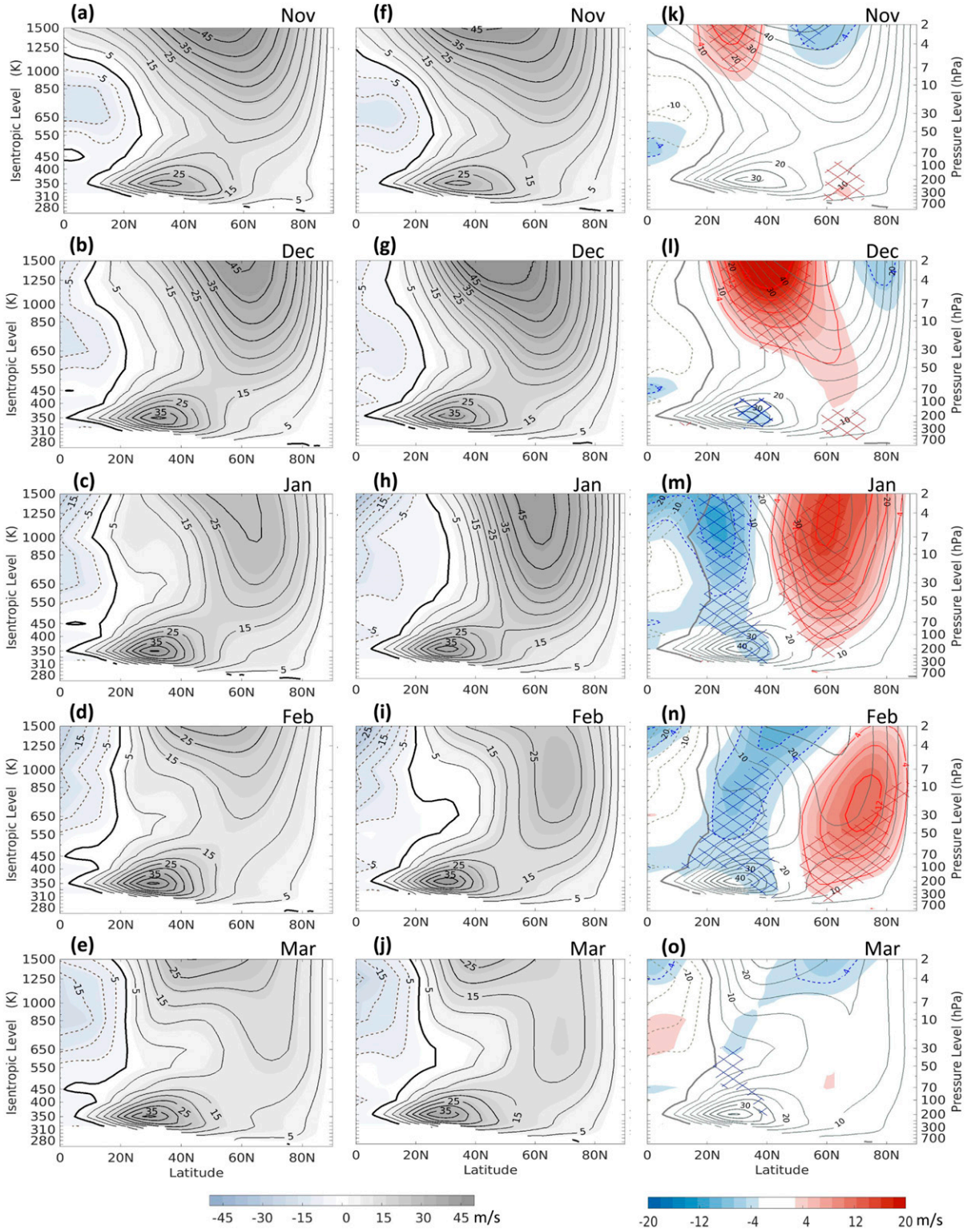

FIG. 2. (a)–(e) Latitude–height section of monthly mean zonal-mean zonal wind $\overline{u}$ from November to March for the narrow-jet regime. Solid and dashed lines indicate westerly and easterly winds. Bold solid lines are the subtropical zero-wind line. (f)–(j) As in (a)–(e), but for the wide-jet regime. (k)–(o) Composite differences (wide − narrow) of $\overline{u}$ (color shaded) and climatological zonal winds (gray contours). Crosshatching specifies statistical significance at $p \leq 0.05$.

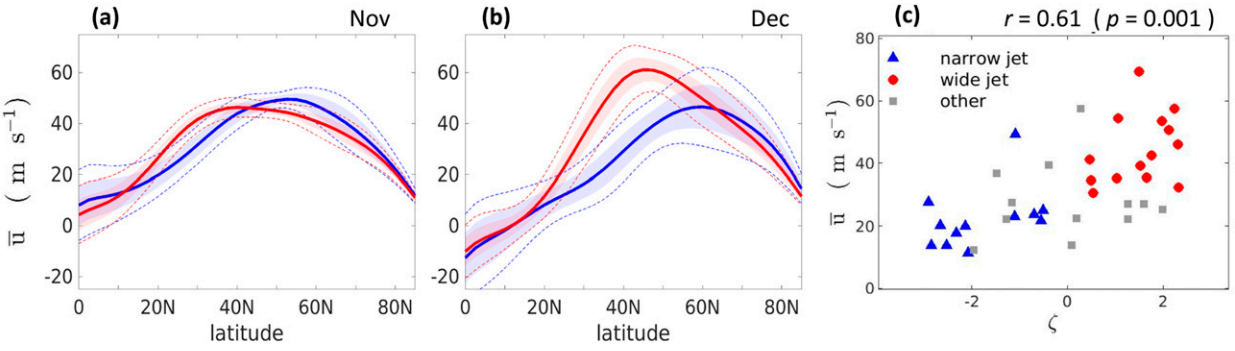

FIG. 3. Latitude profiles of zonal-mean zonal wind $\overline{u}$ at 1500 K for (a) November and (b) December. Solid blue (red) lines are averages for the narrow (wide) jet regime. Shading indicates the 95% confidence intervals of the composite averages while dashed lines are one standard deviation. (c) Scatterplot between December-areal-averaged zonal-mean zonal wind $\overline{u}$ at 25°–45°N, 1500 K and the regime index ζ.

to the climatological behavior of anticyclone frequency in the NH winter that tilts westward with altitude, maximizing over the North Pacific in the lower stratosphere but over the North Atlantic in the upper stratosphere (Harvey et al. 2002). In this context, Figs. 4a–d implies a more zonally symmetric polar vortex and reduced stratospheric anticyclonic disturbance in December in the wide-jet regime.

The temperature differences in the upper stratosphere are marked by cold anomalies (up to −10 K) at 0°–120°E, 50°–80°N with warm differences (~2 K) in the subtropics at 0°–20°N (Fig. 4e). Negative temperature differences are also found in the middle to lower stratosphere though the magnitude becomes smaller (−6 K at 450 K) and the signal is more confined to northeast Asia (Figs. 4f–h). Thus, the stratospheric temperature response is vertically coherent, extending from the upper stratosphere to the lower stratosphere. These temperature differences are not associated with SSWs because each regime has only one major SSW in December (see Fig. 1 and Table 1). They are more likely linked to the upper stratosphere/lower mesosphere (USLM) disturbances described by Greer et al. (2013, 2015). The USLM temperature disturbances occurred ~2.3 times per winter on average with up to 60 K increase in temperature at 0°–120°E, 50°–80°N near the stratopause (Greer et al. 2013), which coincides with the region of significant negative temperature differences (Fig. 4e). In this context, Fig. 4e implies enhanced (reduced) USLM disturbances in December for the narrow (wide) jet regime.

Figure 2 suggests that the differences in zonal winds between the two flow regimes in the lower stratosphere maximize in mid-to-late winter, that is, January–February. To understand how these differences vary longitudinally, Figs. 5a and 5b shows the stereographic plot of January–February-averaged zonal winds u at 450 K (~85 hPa) for the narrow- and wide-jet regimes. Note that these diagnostics are derived up to two months after the definition of the regime indices and thus provide potential predictive capability.

The midlatitude westerly jet over the North Atlantic is 8–10 m s^{-1} stronger in the wide-jet regime than the narrow-jet regime at 450 K. Conversely, over the North Pacific at 150°E–150°W, u at the exit region of the subtropical westerly jet is significantly weaker (by ~2–5 m s^{-1}). The differences in u are nearly annular at high latitudes with westerly differences at 60°–80°N, while relatively weak easterly differences are found at 20°–40°N over the two ocean basins (Fig. 5c). This annular pattern corresponds to an anomalously deeper polar vortex in the high latitudes and weaker winds in the surfzone during the wide-jet winters.

Figure 5d shows the scatterplot between the regime index ζ and zonal-mean zonal wind $\overline{u}$, area-averaged over the latitude band of 50°–70°N, 350–550 K in January–February. $\overline{u}$ is positively correlated with the flow index ζ with $r = 0.51$ ($p < 0.01$). The average wind speed in this region is 19 m s^{-1} for the wide-jet regime but only 13.8 m s^{-1} for the narrow-jet regime and the difference (5.5 m s^{-1}) amounts to nearly 33% of the climatological $\overline{u}$ at 50°–70°N, 350–550 K in January–February. We note that the correlation is closely linked to the occurrence of the major SSWs with seven major SSWs occurring in the narrow-jet winters (see Fig. 5d) but only three in the wide-jet regime. Interestingly, the majority of major SSWs in the narrow-jet regime (five of the seven) were of displacement type (Butler et al. 2015) while the majority of major SSWs in the wide-jet regime were of split type (two of the three).

Since the flow regimes are defined based on November–December standard deviation of the EPV in the upper stratosphere at 1500 K, Fig. 5 suggests a measure of predictability for the lower-stratospheric circulation from the early winter upper stratosphere, which could be useful for seasonal forecasts.

d. *Tropospheric responses*

Mid-to-late winter [January–February (JF)] tropospheric responses to the flow regimes defined using November–December EPV data in the upper stratosphere at 1500 K are studied in this section.

Figures 6a and 6b show the anomalies of JF-mean zonal winds u at 300 K (~700 hPa) for the narrow- and wide-jet regimes. The separate composite anomalies (from the climatological mean) rather than the composite differences are shown because their spatial distributions do not always have the opposite sign in a given geographical location, which implies the

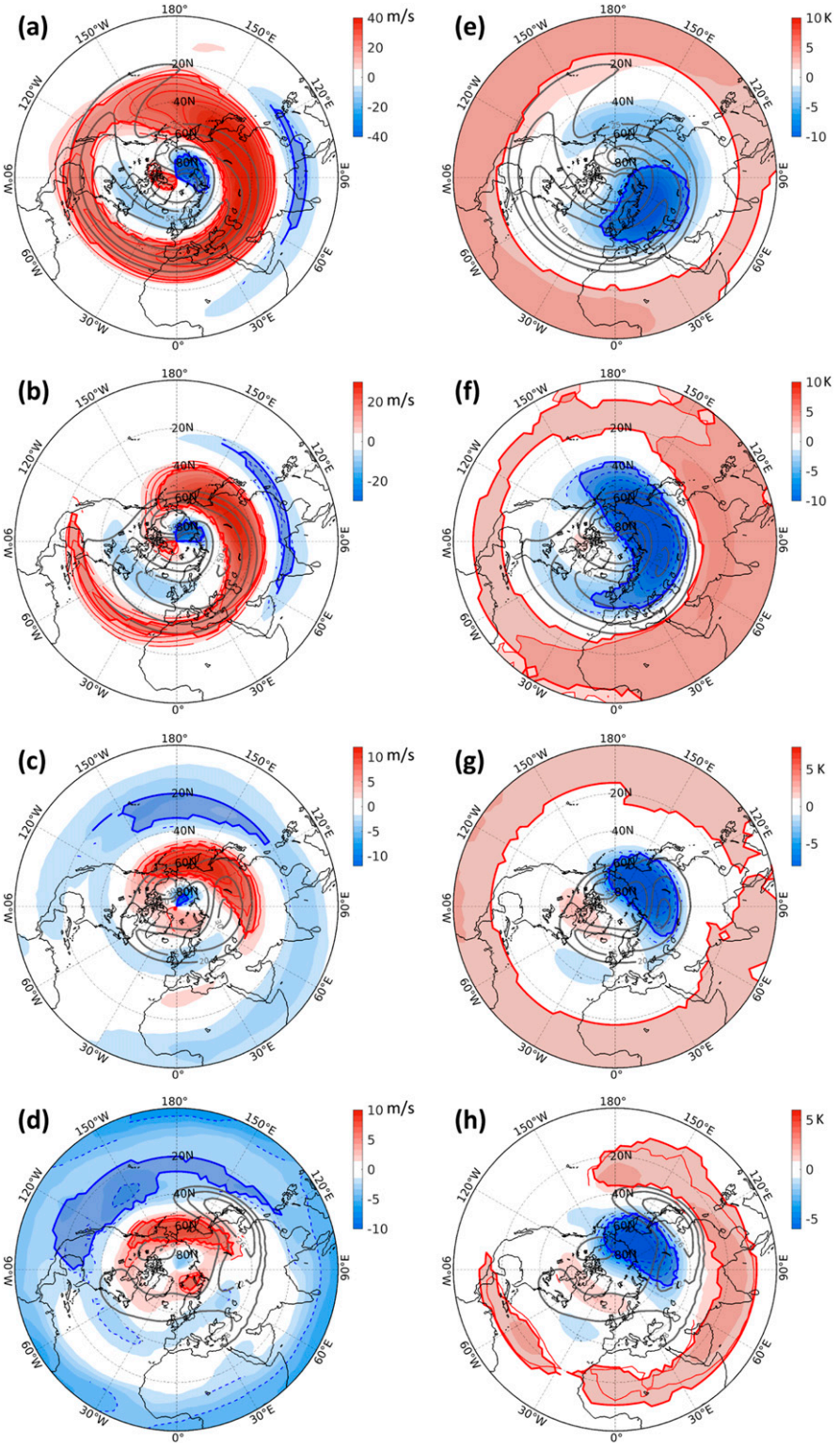

FIG. 4. Stereographic maps of composite differences (wide − narrow; color shaded) of December (a)–(d) zonal winds and (e)–(h) temperature at 1500 K in (a) and (e), 850 K in (b) and (f), 550 K in (c) and (g), and 450 K in (d) and (h). Regions enclosed by solid red and blue lines specify statistical significance at $p \leq 0.05$. Climatological December u are denoted by the gray-contours.

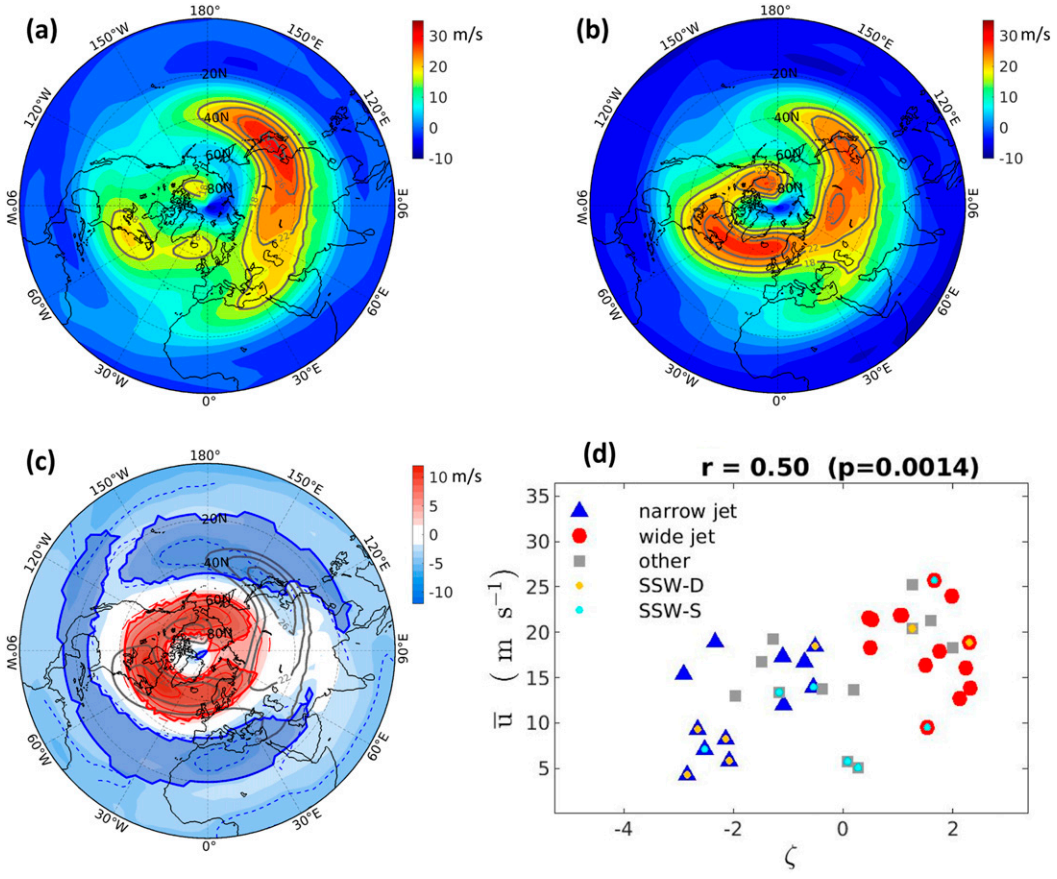

FIG. 5. (a) Stereographic plot of JF-averaged zonal wind at 450 K for the narrow-jet regime. Contours are from 18 to 26 m s^{-1} with an interval of 4 m s^{-1}. (b) As in (a), but for the wide-jet regime. (c) Composite differences (wide − narrow; shaded) with contour interval of 2 m s^{-1}. Regions enclosed by solid red and blue lines specify statistical significance at $p \leq 0.05$. Gray contours indicate climatological JF mean u. (d) Scatterplot between JF-areal-averaged zonal-mean zonal wind $\overline{u}$ at 50°–70°N, 350–550 K and the regime index ζ.

presence of nonlinear interactions and could possibly be related to the type of (split or displacement) SSW (Butler et al. 2015), although this would require further investigation.

The u anomalies for the narrow-jet regime are statistically significant over the North Atlantic, where the effect is marked by alternating positive-negative-positive u anomalies with westerly anomalies (~3 m s^{-1}) at 15°–80°W, 25°–40°N, easterly anomalies (~6 m s^{-1}) at 0°–90°W, 45°–65°N, and westerly anomalies (~4 m s^{-1}) at 70°–85°N. These anomalies suggest a southward shift of, or a broader-than-normal Atlantic westerly jet (Fig. 6a), which, to a large extent, resembles the negative phase of the NAO (Scaife et al. 2016). Weaker but statistically significant easterly anomalies (1–2 m s^{-1}) are also found over subtropical Eurasia at 45°–90°E, 20°–30°N.

The u anomalies in the wide-jet regime are statistically significant over the North Pacific with easterly anomalies (−4 m s^{-1}) near the exit region of the Pacific westerly jet at 145°E–140°W, 30°–45°N. Statistically significant westerly anomalies (~3 m s^{-1}) are found to scatter around a latitude band near 50°–65°N that is centered over northern Canada (Fig. 6b), signifying a weaker, poleward shifted tropospheric westerly jet (Thompson and Wallace 1998). Westerly anomalies (~1 m s^{-1}) are found in the subtropics at 45°–90°E, 20°–35°N.

The temperature anomalies in the narrow-jet regime are characterized by warm anomalies in the Arctic over northern Canada, the Labrador Sea, and Greenland at 0°–120°W, 65°–90°N (~5 K) and over subtropical Eurasia at 10°–100°E, 20°–35°N (~3 K, Fig. 6c). Cold anomalies (up to −3 K) are found over northern Europe at 30°–70°E, 35°–45°N and over eastern North America at 50°–80°W, 40°–50°N, implying an increased probability for cold-air outbreaks over the east coast of North America and northern Europe in the narrow-jet regime. The temperature anomalies in the wide-jet regime are marked by warm anomalies (up to 5 K) over the North Pacific at 150°E–130°W, 40°–60°N and cold anomalies (up to −3 K) over northern Canada and over subtropical to midlatitude Eurasia at 15°–90°E, 25°–45°N (Fig. 6d). Thus, southern Europe (the Aleutian low) was colder (warmer) than average during the wide-jet winters.

Figures 7a and 7b shows the climatology and the composite differences in the JF-mean amplitude of high-pass filtered (periods < 10 days) meridional winds at 300 K, which is

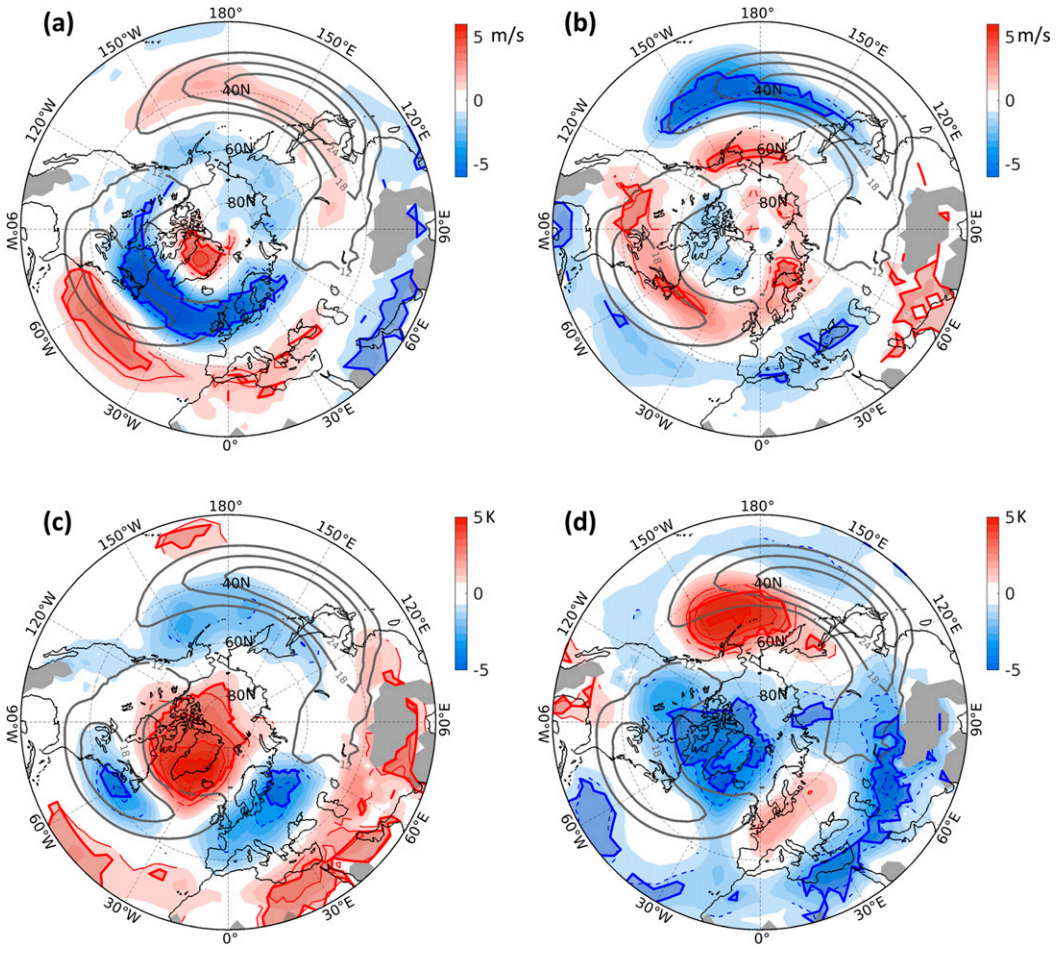

FIG. 6. (a) Stereographic plot of JF-averaged zonal wind anomalies (color shaded, with contours from 2 to 6 m s^{-1} and an interval of 1 m s^{-1}) at 300 K for the narrow-jet regime. Regions enclosed by solid red and blue lines specify statistical significance at $p \leq 0.05$. Dark-gray-shaded regions have no data as the θ level intersects with the ground there. (b) As in (a), but for the wide-jet regime. (c),(d) As in (a),(b), but for temperature. Climatological JF-mean zonal winds are shown as gray contours (12–24 m s^{-1} with an interval of 4 m s^{-1}).

a measure of storm-track intensity (Chang et al. 2002). Climatologically, high-frequency $|v'|$ peaks over the North Atlantic (Fig. 7a). Thus, the storm track is strongly coupled to the NAO. The statistically significant positive differences scattered near 60°W–60°E, 55°–65°N suggest that the storm track is shifted poleward and extends farther eastward into northern Europe in the wide-jet regime (Fig. 7b).

Figures 7c and 7d show the climatology and composite differences in the JF-mean amplitude of the high-pass filtered (periods < 10 days) temperature at 300 K. Climatologically, high-frequency $|T'|$ maximizes downstream of the North Pacific westerly jet and all the way along the North Atlantic westerly jet. The statistically significant positive and negative $|T'|$ differences downstream of the North Atlantic westerly jet at 10°–60°E, 55°–75°N and at 5°–25°E, 35°–50°N are consistent with a poleward shifted storm track in the wide-jet regime (Fig. 7d). Figure 7d also indicates that synoptic-scale weather pattern over northern Europe and the east coast of North America were more variable than normal, that is, with more frequent weather extremes, in the wide-jet regime. Conversely, more frequent weather extremes are expected over southwest Europe in the narrow-jet regime.

e. *Linkage to other atmospheric modes*

In this section, we aim to address the following questions: 1) Is the regime index ζ somehow linked to the NAM? 2) To what extent does the regime index ζ project onto the regional climate modes in the troposphere, such as the NAO, the AO, and the Pacific–North American teleconnection pattern (PNA)?

Figure 8a shows the correlations between the regime index ζ and the monthly NAM in the time–pressure cross section from October to March and from 1000 to 1 hPa. At a given pressure level and for a given month, the NAM is defined by $-(\overline{Z}_{65-90N} - \overline{Z}_{global})$, where $\overline{Z}_{65-90N}$ is the zonally averaged geopotential height poleward of 65°N and $\overline{Z}_{global}$ is the global-averaged geopotential height. This is the simplified version of NAM derivation proposed by Baldwin and Thompson (2009) and used by Gerber and Martineau (2018) and others.

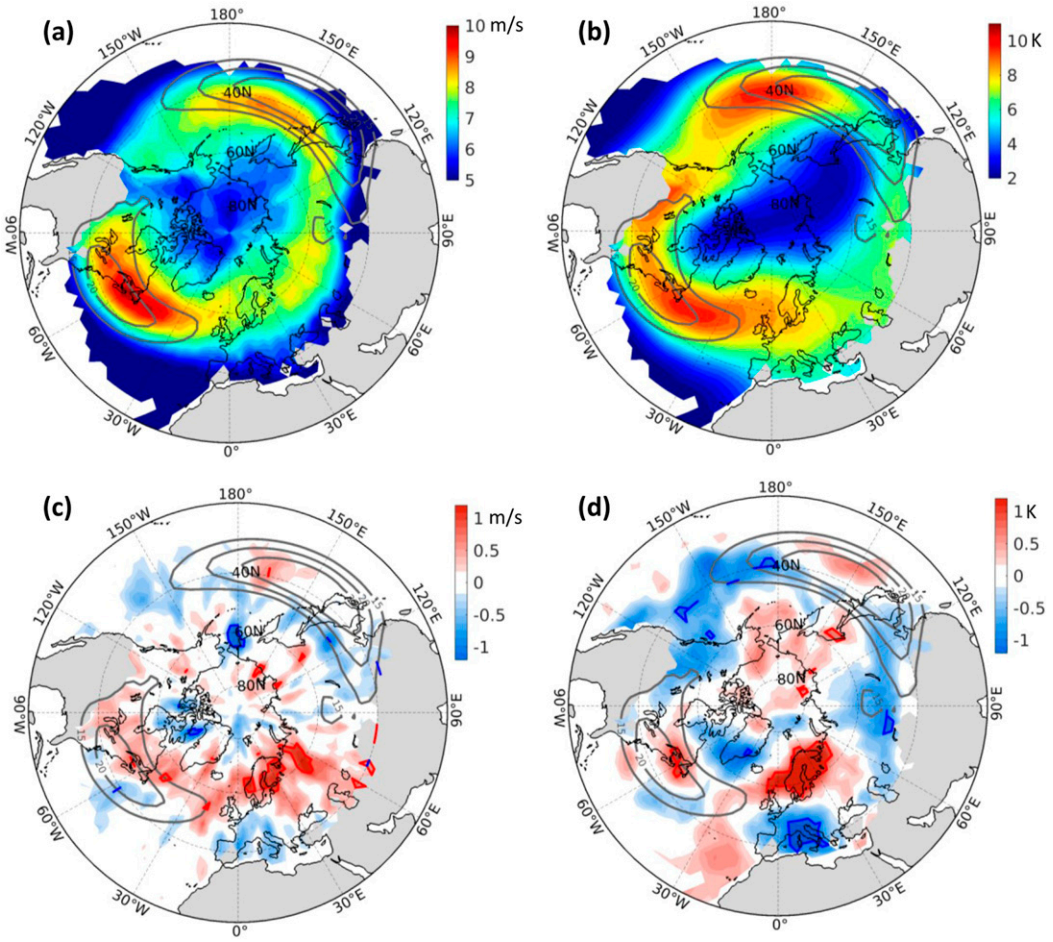

FIG. 7. (a),(c) Stereographic plot of JF-averaged amplitude of high-pass filtered meridional wind speed $|v'|$ (m s^{-1}; color shaded) for the narrow- and wide-jet regimes at 300 K. (c) Composite differences (wide − narrow) (m s^{-1}; shaded). Gray contours, statistically significant regions, and gray-shaded regions are same as Fig. 6. (b),(d) As in (a) and (c), but for temperature (K).

Statistically significant correlations between the regime index ζ and the NAM are found at 300–850 hPa and at 30–50 hPa in October–December (OND), indicating that characteristics of the early winter NAM in both the troposphere and lower-stratospheric are reflected in the ζ regime definition. A downward progression of the ζ correlation from 7 to 200 hPa is evident from December to February. The maximum correlation coefficient between ζ and the monthly NAM is 0.44 in January in the lower stratosphere at 70 hPa and the correlation is still significant at the 95% level in February. This suggests that knowledge of the regime index derived using November–December data in the upper stratosphere can provide predictability of the lower-stratospheric circulation at least 2 months ahead. A lack of statistical significance above 7 hPa suggests that the regime index ζ is not simply a replica of the NAM in the upper stratosphere.

It has been shown that the lower stratosphere has the longest memory, and the lower-stratospheric NAM has the largest impact on the troposphere (Baldwin and Dunkerton 2001; Scott and Polvani 2004; Martineau et al. 2018). As a comparison, Fig. 8b shows the corresponding plot but the regime index ζ is replaced by the November–December-averaged NAM at 50 hPa. Not surprisingly, the NAM is well correlated with itself during the definition months of November–December with $r >$ 0.5 throughout the depth of the atmosphere, an illustration of the in-month vertical connectivity of the stratosphere–troposphere circulation. Comparison of the two figures shows that despite the significant correlation of ζ with the NAM in the middle stratosphere (as shown in Fig. 8a), the regime index ζ is not simply an alternative measure of the NAM in the middle to lower stratosphere. In contrast to the ζ correlations that remain statistically significant until February at 50–200 hPa, correlations with the November–December NAM are only statistically significant until January (for all pressure levels). Figure 8 suggests that the regime index ζ provides more potential predictability than the November–December NAM. In fact, it provides extended predictability to the NAM in the lower stratosphere until February.

Table 2 shows the correlation coefficients between the regime index ζ and the three regional tropospheric modes, that is,

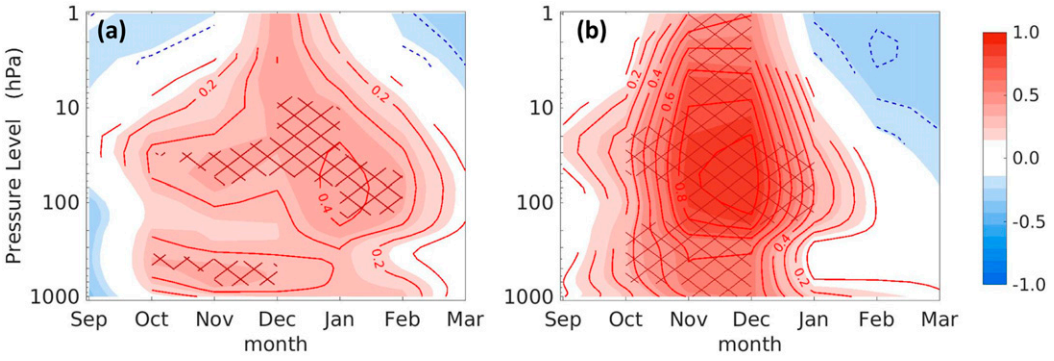

FIG. 8. (a) Correlations between the regime index ζ and the monthly NAM in time–pressure cross section from September to March and from 100 to 1 hPa. Crosshatching specifies statistical significance at $p \leq 0.05$. (b) As in (a), but ζ is replaced by the November–December-averaged NAM at 50 hPa.

the NAO, the AO, and the PNA for two months and three months running averages. No significant correlations can be found in early winter, implying that the regime index ζ is not simply an alternative measure of either of these tropospheric indices. However, ζ is most significantly correlated with the DJF-averaged AO, with the PNA in December–January (DJ), and with the NAO in January–February. The regime index ζ accounts for 22% of the variance in the December–January PNA, 23% of the variance in the December–January AO, and 12% of the variance in the January–February NAO. These results demonstrate that the regime index ζ can provide predictability for tropospheric variability in mid-to-late winter. The correlations with the PNA and the NAO are of the opposite sign, consistent with the zonally asymmetric signal in zonal winds and temperatures (see Fig. 6). Moreover, the impact may initialize in the North Pacific since the correlation with the PNA leads that with the NAO by one month, but this would require further investigation.

f. The role of RWB

In this section, we examine the upper-stratospheric waveguide in early winter and the role of RWB (McIntyre and Palmer 1983; Hitchman and Huesmann 2007).

Figures 9a and 9b show the composites of meridional gradient of the EPV (i.e., P_ϕ) for the narrow- and wide-jet regimes at 1500 K during December, when the upper-stratospheric signal is largest. Weaker but similar results can be obtained in November, but the signals become insignificant after mid-January (not shown). In agreement with previous studies (e.g., Harvey et al. 2002; Manney et al. 2008), the winter upper stratosphere is effectively separated into three dynamically meaningful regions, the westerly jet that spirals from the subtropics to polar latitudes, the surfzone at 10°–40°N and the vortex core at 65°–90°N. The P_ϕ maximizes along the westerly jet and is a minimum in the surfzone and the vortex core. The three regions are separated by a stepwise change of P_ϕ at the edge of the westerly jet, which can be seen in the narrow- and wide-jet regimes. For the narrow-jet regime, however, the necessary condition for instability is met primarily near the AH at 120°E–150°W, 30°–60°N (Fig. 9a). In contrast, for the wide-jet regime, the instability condition of $P_\phi \leq 0$ is met primarily in the subtropics at 15°–40°N, and over an extended longitude band of 90°W–120°E (Fig. 9b). A very sharp increase of P_ϕ (from ≤ 0 to 15×10^{-10} K m^2 kg^{-1} s^{-2}) is found equatorward of the westerly jet at 90°W–120°E, 25°–40°N in association with the wide-jet regime (Fig. 9b).

The composite differences (Fig. 9c) confirm a significant enhancement of P_ϕ at the equatorward flank of the climatological westerly jet in the wide-jet regime, which is accompanied by significant reduction of P_ϕ in both the surfzone and the vortex core. These results together with Fig. 2 suggest an upper-stratospheric westerly jet that extends farther equatorward in the wide-jet regime and has a sharper edge, which is known to be an indication of RWB (Waugh and Dritschel 1999; Hitchman and Huesmann 2007).

Figures 9d and 9e show the corresponding December composites of ϑ, a measure of high-frequency (periods < 10 days) variability in the background waveguide [see Eq. (1)]. The ϑ maximizes over the Arctic within the vortex core in the narrow-jet regime (Fig. 9d) but over East Asia at 90°E–180°, 40°–65°N (Fig. 9e) in the wide-jet regime. The ϑ minimizes in the subtropical surfzone with close to zero values there in the

TABLE 2. Correlation coefficients between the regime index ζ and the NAO, the AO, and the PNA for a range of seasonal averages. Numbers in bold type with ** are statistically significant at $p < 0.01$. Italic numbers with * indicate the correlation is only significant at $p < 0.05$.

	ON	ND	DJ	JF	FM	OND	NDJ	DJF	JFM
NAO	−0.24	0.18	0.23	*0.35**	0.21	0.15	0.22	*0.33**	*0.34**
AO	0.29	0.32	**0.41****	**0.42****	0.23	*0.37**	**0.42****	**0.45****	*0.35**
PNA	−0.24	−0.19	**−0.47****	−0.30	−0.28	*−0.37**	*−0.37**	*−0.39**	*−0.31**

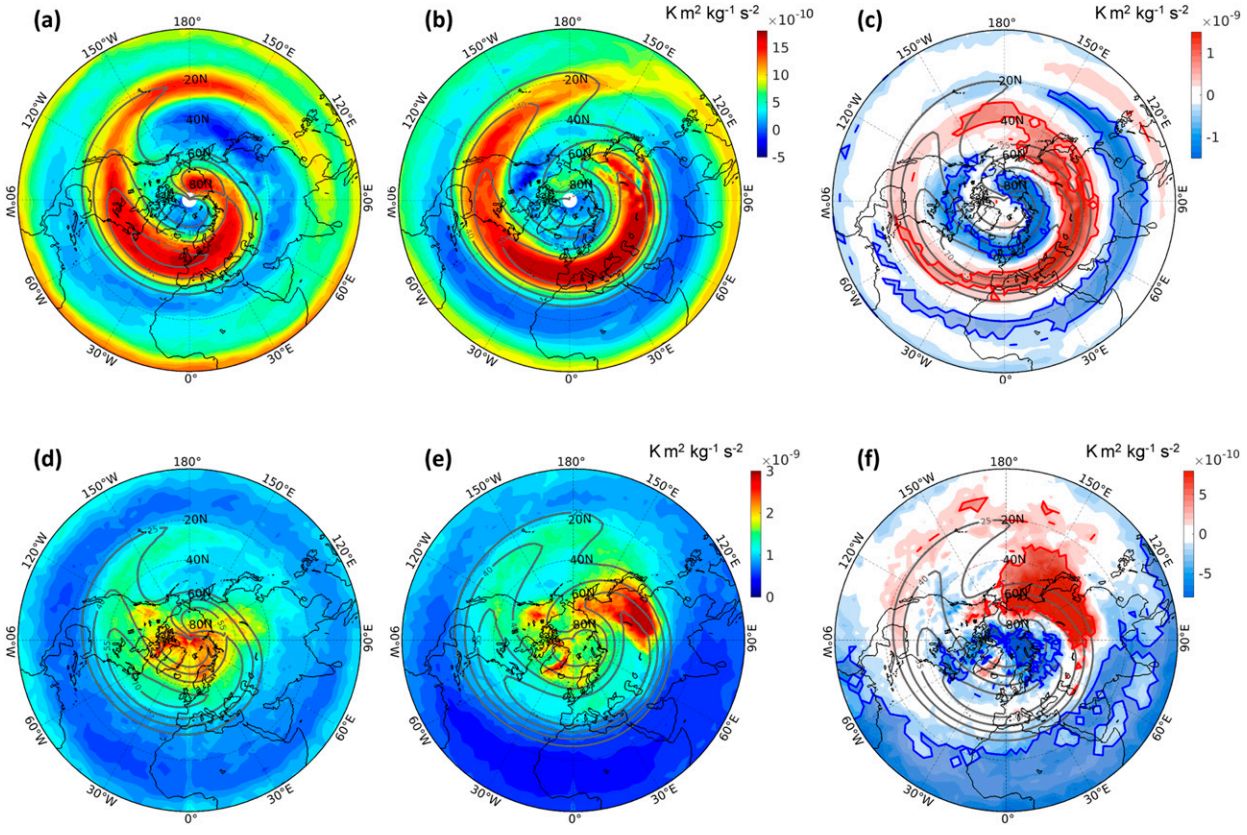

FIG. 9. (a) Stereographic plot of December meridional EPV gradient P_ϕ (K m^2 kg^{-1} s^{-2}; shaded) and zonal winds u (contoured from 25 to 70 m s^{-1} with an interval of 15 m s^{-1}) at 1500 K for the narrow-jet regime. (b) As in (a), but for the wide-jet regime. (c) Composite difference (wide − narrow). Climatological December u is contoured. Regions enclosed by solid red and blue lines specify statistical significance at $p \leq 0.05$. (d)–(f) As in (a)–(c), but for high-frequency (<10 days) variability of the waveguide ϑ [K m^2 kg^{-1} s^{-1}; Eq. (1)].

wide-jet regime (Fig. 9e), indicating reduced small-scale mixing. Composite differences between the wide-jet and the narrow-jet regimes are statistically significant over East Asia, the Arctic, and the subtropical surfzone (Fig. 9f).

Quasi-stationary PRWs from the troposphere are predominantly low frequency with a period > 10 days (Matsuno 1971; Harvey and Hitchman 1996; Harvey et al. 2002), which cannot directly cause high-frequency variation in the background waveguide. Localized high-frequency disturbances to the supposedly slowly varying waveguide signify wave–wave interactions (O'Neill and Pope 1988; Sivan et al. 2016). In light of Fig. 4, the enhanced high-frequency disturbances to the background waveguide over East Asia at 90°E–180°, 40°–65°N in the wide-jet regime indicate localized wave–wave interaction that acts to hinder the development of the AH downstream. Thus, Fig. 9 implies that the upper stratosphere of the narrow-jet regime is characterized by stronger disturbances of quasi-stationary PRWs that successfully penetrate and build up the AH in early winter while the wide-jet regime has an equatorward-shifted polar vortex and a less-well-developed AH.

Figures 9a–c indicate RWB may play a major role in the wide-jet regime winters because of the noticeable sharpening of the westerly jet. We now explore the vertical structure and temporal evolution of RWB and examine how they differ between the two flow regimes.

Figure 10 shows two-month running averages of the zonally averaged frequency of overturning PV contours $\overline{\gamma}$ for the narrow-jet (Fig. 10a–d) and wide-jet (Figs. 10e–h) regimes and their corresponding differences (Figs. 10i–l) from October–November (ON) averages to January–February averages. The analysis starts in October–November because changes in RWB appear to lead the circulation anomalies.

For both the narrow- and wide-jet regimes, the climatology of $\overline{\gamma}$ is marked by regions with infrequent RWB (<15 days per two months) near the two westerly jets, at the equator and in the subtropical middle to lower stratosphere. The $\overline{\gamma}$ maximizes in the stratospheric surfzone at 20°–45°N and the extratropical upper troposphere and lower stratosphere (up to 27 days per two months). Regions with relatively large values of $\overline{\gamma}$ indicate mixing and thus more frequent RWB.

Modulation of RWB frequency starts in the upper stratosphere as well as in the midlatitude troposphere, with RWB occurring more frequently in the wide-jet regime at 40°–55°N, 1250–1500 K (by 3 days per month on average) but less frequently near the tropopause region at 60°–70°N, 300–400 K (by 2 days per month on average) than in the narrow-jet regime (Figs. 10a,e,i). The region of positive $\overline{\gamma}$ differences in the upper

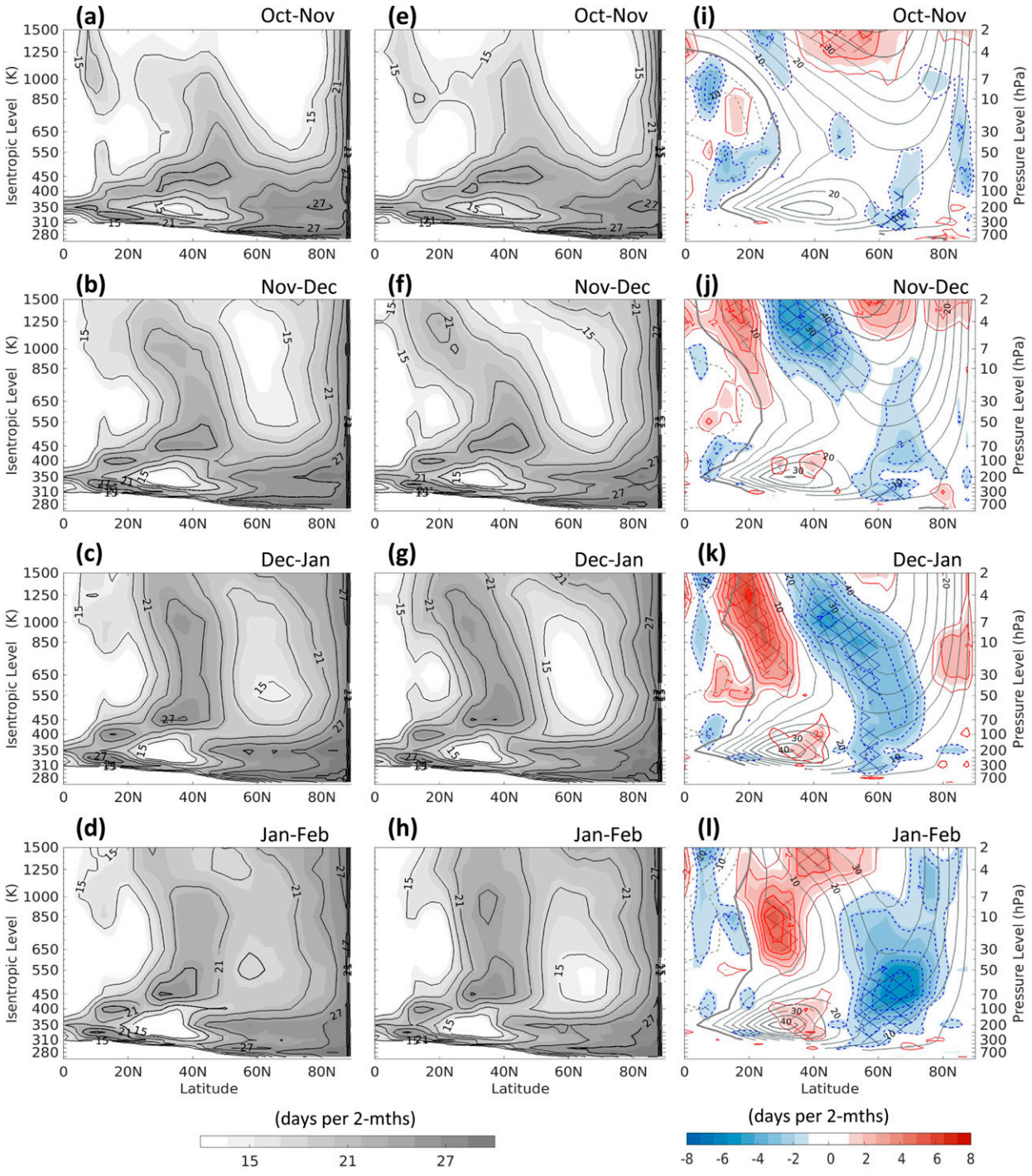

FIG. 10. (a)–(d) Latitude–height section of two-month running mean (from October–November to January–February) of reversal frequency of meridional EPV gradients $\overline{\gamma}$ (in days per two months) for the narrow-jet regime. Contours are 15–27 days with an interval of 3 days. Regions with large (small) values of $\overline{\gamma}$ are shaded in gray (white) to highlight the surfzone (the polar vortex edge). (e)–(h) As in (a)–(d), but for the wide-jet regime. (i)–(l) Composite differences (wide − narrow) of $\overline{\gamma}$ (shading) with climatological zonal winds (contours) and subtropical zero-wind line (thick solid line). Crosshatching specifies statistical significance at $p \leq 0.05$.

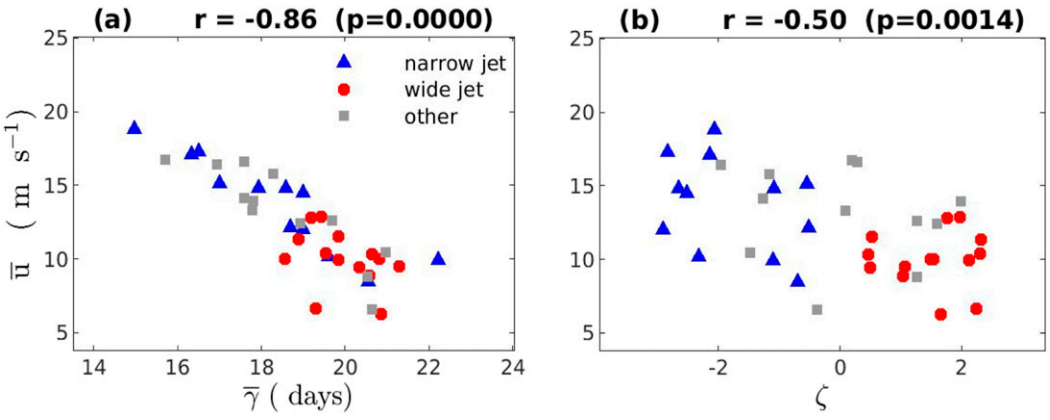

FIG. 11. (a) Scatterplot between JF-mean $\overline{u}$and $\overline{\gamma}$, both averaged over stratospheric surfzone at 20°–40°N, 350–1500 K. (b) As in (a), but $\overline{\gamma}$ is replaced by the regime index ζ.

stratosphere moves poleward in November–December and weakens thereafter. The region of negative difference near the tropopause moves slightly equatorward, extends upward into the stratosphere where a similar region of negative difference has developed in the upper stratosphere (November–December), and this negative feature persists across the winter (Figs. 10i–l). The upper-stratospheric negative region forms part of a dipolar response (from November to December) with a corresponding positive difference in the subtropics, indicating that the surfzone in this height region is shifted more equatorward in the wide-jet regime (as is also the upper-stratospheric polar vortex, see Figs. 9a–c). The differences start in the upper stratosphere around November–December (Figs. 10b,f,j) and then extend downward in December–January (Figs. 10c,g,k). Also, the positive $\overline{\gamma}$ differences are located near the subtropical zero wind line at 15°–35°N and the negative $\overline{\gamma}$ differences are positioned on the equatorward flank of the polar vortex at 30°–55°N (Figs. 10j–l). Thus, an increase in RWB frequency in the subtropics is accompanied by a decrease of RWB frequency at the polar vortex edge. This suggests that RWB plays a predominant role in the wide-jet regime while Matsuno-type wave absorption dominates in the narrow-jet regime. In the lower stratosphere and upper stratosphere, an anomalous equatorward shift of RWB is found in the wide-jet regime (Figs. 10c,g,k). The stratospheric polar vortex becomes anomalously stronger during the wide-jet regime in middle winter as wave activity near the tropopause shifts equatorward, thus away from the polar vortex edge. In January–February, the $\overline{\gamma}$ contours along the polar vortex edge become indistinguishable from those in the surfzone for the narrow-jet regime (Fig. 10d) but remains distinct in the lower stratosphere for the wide-jet regime (Fig. 10h).

Taking the contour of $\overline{\gamma}$ = 15 days per 60 days as a useful reference value, the midwinter polar vortex does not extend below 450 K in the narrow-jet regime but reaches 400 K in the wide-jet regime (Figs. 10c,d vs Figs. 10g,h). Thus, deeper penetration of the polar vortex in mid–late winter accompanies an equatorward shift of the surfzone and less frequent RWB on the equatorward flank of the polar vortex in the wide-jet regime. The same effect can also be seen by comparing Fig. 2d and Fig. 2i. In contrast, RWB encompasses the entire extratropical NH in the narrow-jet regime and is accompanied by an earlier weakened polar vortex (also see Fig. 2). These regime behaviors of RWB are consistent with Manney et al. (1994) who found that a stronger and deeper-than-average PNJ was closely related to reduced mixing across the polar vortex edge. They are also consistent with idealized model simulations in which reduced upward wave propagation and more frequent upper-level RWB were found to be associated with a vortex that increases in area with height (Waugh and Dritschel 1999; Polvani and Saravanan 2000).

To appreciate the role of RWB in the stratospheric surfzone and the differences between the two flow regimes, Fig. 11a shows the relationship between zonal-mean zonal wind $\overline{u}$ and $\overline{\gamma}$ averaged over 20°–40°N, 350–1500 K for January–February. Climatologically, $\overline{u}$ and $\overline{\gamma}$ in the stratospheric surfzone is highly correlated ($r = -0.85$). The negative correlation between $\overline{u}$ and $\overline{\gamma}$ is expected because RWB acts to mix the high EPV air from the polar vortex edge with the low EPV air in the subtropics. The RWB slows down the background winds in the surfzone. A very strong linear relationship between $\overline{u}$ and $\overline{\gamma}$ holds for the narrow-jet regime ($r = 0.91$, $p < 0.001$). In contrast, the wide-jet winters are confined to the sector where $\overline{\gamma} > 18$ days and $\overline{u} \leq 13\,\mathrm{m\,s^{-1}}$ and there is noticeably more spread and no significant correlation between $\overline{u}$ and $\overline{\gamma}$ in the stratospheric surfzone ($r = 0.39$, $p = 0.17$). The lack of linear correlation is a good indication of nonlinear wave breaking. It is because, unlike simple wave absorption, nonlinear wave breaking involves a complex cycle of absorption–reflection–overreflection within the surfzone, induced by localized overturning of the PV contours between the zero-wind line and the polar vortex edge (Killworth and McIntyre 1985) so that the relationship between $\overline{u}$ and $\overline{\gamma}$ would change and even reverse, depending on the stage of the absorption or reflection. Nevertheless, the net effect of overturning PV contours due to nonlinear wave breaking is irreversible mixing, and thus an overall reduction of the zonal winds in the stratospheric surfzone in the wide-jet winters.

To demonstrate that the upper-stratospheric flow regime plays a significant role in modulating wave breaking in the

surfzone, $\overline{\gamma}$ in Fig. 11a is replaced by the regime index ζ while $\overline{u}$ remains unchanged and the result is shown in Fig. 11b. It is evident that the surfzone averaged $\overline{u}$ at 20°–40°N and 450–850 K in January–February is negatively correlated with the regime index ζ that is defined in November–December ($r = -0.5$, $p < 0.01$). This negative correlation exists mainly because the zonal winds in the stratospheric surfzone are significantly weaker for the wide-jet regime. Thus, Fig. 11b confirms that the upper-stratospheric variability in November–December modulates the zonal winds in the surfzone, and thus stratospheric RWB in mid-to-late winter.

4. Conclusions and discussion

An early winter regime index ζ is constructed for the NH winter based on the leading empirical orthogonal function (EOF1) of the November–December standard deviation of daily Ertel's potential vorticity at 1500 K (~42 km). The EOF1 is manifested by a seesaw pattern in the vicinity of the upper-stratospheric westerly jet and captures 40% of intraseasonal EPV variability in the NH near the stratopause. The difference between the normalized, areal-averaged upper and lower 50% percentiles of the EOF1 effectively defines the regime index ζ (Fig. 1).

This new index ζ provides a geometric identification of the structure of the stratospheric polar vortex and regulates the vortex development later in the winter (Figs. 2 and 3). The regime index ζ provides information of the strength, latitudinal extent, and, in particular, seasonal evolution of the stratospheric polar vortex. The characterization provided by ζ is useful because idealized high-resolution vortex simulations have demonstrated that both upward wave propagation and RWB are sensitive to the initial vertical structure and latitudinal extent of the polar vortex (Waugh and Dritschel 1999; Polvani and Saravanan 2000). Using the CFSR/CFSv2 reanalysis datasets, results are provided to show that the vortex weakens at least one month earlier in the narrow-jet regime than the wide-jet regime. The weakening is associated with strong PV mixing across the extratropical stratosphere, especially at the polar vortex edge (Figs. 10c,d). In contrast, the wide-jet regime is associated with a stronger and wider upper-stratospheric westerly jet in early winter and the jet core shifts poleward and extends deeper into the lower stratosphere in mid-to-late winter (Fig. 2). The vertical coupling within the stratosphere in the two regimes is zonally asymmetric, largely confined to the North Pacific and East Asia, and statistically significant since December (Fig. 4). The most persistent circulation anomalies are detected in the lower stratosphere, where nearly annular zonal wind anomalies are found in January–February (Fig. 5c). The regime index ζ also regulates the SSWs, with more major SSWs occurring in the narrow-jet regime than the wide-jet regime in January–February (7 vs 3, Fig. 5d). Also, most of the January–February major SSWs in the narrow-jet regime are of displacement type (5 out of 7). The opposite holds true for the wide-jet regime as two of the three January–February major SSWs are of split type.

Our analysis demonstrates a predictive capability of the regime index ζ for the tropospheric circulations in mid-to-late winter, including the regional indices, such as the PNA, the AO, and the NAO (Figs. 6–8 and Table 2). The regime index ζ generally leads the tropospheric anomalies by one to two months and correlates most strongly with the PNA ($r = 0.47$) in December–January. Spatially, the narrow-jet anomalies are confined primarily to the North Atlantic and resemble the negative phase of the NAO (Fig. 6b). This response is consistent with previous studies that have found tropospheric sensitivity to stratospheric variability primarily confined to the Atlantic basin in association with a weakened polar vortex state in the lower stratosphere (Charlton-Perez et al. 2018; Maycock et al. 2020). Increased cold outbreaks are likely to occur more frequently in the northwest of Europe and east coast of North America in the narrow-jet regime in mid-to-late winter. In contrast, the wide-jet anomalies project most significantly over the North Pacific with a weaker-than-average westerly jet and a warmer-than-average Aleutian low. Nonlinear processes or perhaps the type of SSW (split or displaced) may also play a role in the zonally asymmetric signal seen in the troposphere at 300 K since there is a greater predominance of displaced (split) SSWs in the narrow (wide) jet regime (Fig. 5d).

The two flow regimes also differ in their impacts on the storm track, especially downstream of the Atlantic westerly jet (Fig. 7). The storm track over western Europe is significantly shifted equatorward (poleward) in the narrow (wide) jet regime (Figs. 7b,d). Also, the synoptic-scale weather systems near the east (west) coast of North America are found to be more (less) variable in the wide-jet regime. These differences in high-frequency variability of meridional winds and temperatures in western Europe and the coast regions of North America may be linked to the occurrences of extreme weather events in these regions.

Comparisons with correlations based on knowledge of the early winter (November–December) 50-hPa NAM confirm that the regime index ζ is not a simple replica of the NAM either in the stratosphere or the troposphere (Fig. 8). More importantly, the regime index ζ has extended predictive capability than the early winter NAM.

In terms of the responsible mechanisms, the RWB analysis suggests the predominance of wave absorption (Matsuno 1971) in the narrow-jet regime but nonlinear RWB (McIntyre and Palmer 1983, 1984) in the wide-jet regime (Figs. 9–11). The different RWB behavior starts in the upper stratosphere in association with a broader-than-average westerly jet in the wide-jet regime (Figs. 2, 3, and 9a–c). Localized, high-frequency variations (periods < 10 days) in the waveguide are detected in the vicinity of the jet exit at 90°–150°E, 35°–60°N, 1500 K in the wide-jet regime, which signify enhanced nonlinear wave interactions (Figs. 9d–f; Sivan et al. 2016). Nonlinear RWB is enhanced in the wide-jet regime with an equatorward-shifted stratospheric surfzone from November–December onward (Figs. 10–11). As a result, the PV gradients at the edge of the stratospheric polar vortex are persistently sharpened from November to February.

Results shown in Figs. 9–11 can be linked to idealized simulations of vortices. Those studies have found that the vertical structure of the vortices plays an important role in determining the characteristics of RWB (Waugh and Dritschel 1999;

Polvani and Saravanan 2000). A reduction in vortex area with altitude leads to focusing of wave activity to the vortex, which amplifies RWB. Conversely, upward wave propagation and RWB are reduced if the vortex area increases with altitude. Waugh and Dritschel (1999) additionally showed that for a vortex with both PV and area increasing with height, a regime exists with persistent RWB occurring in the upper layers where the filaments produced by RWB roll up into a series of small vortices. This may explain the enhanced high-frequency variation in the upper-stratospheric waveguide during the wide-jet winters. The high-frequency variation in upper-stratospheric waveguide may also be related to traveling anticyclones in the midlatitude upper stratosphere (Harvey et al. 2002; Gray et al. 2003).

Processes in the upper stratosphere are known to play an important role in stratospheric dynamics and subsequent downward coupling (O'Neill and Pope 1988; Gray et al. 2020; Lindgren and Sheshadri 2020). This work furthers our current understanding of the stratosphere–troposphere coupling by uncovering the role of the early winter flow regimes in the upper stratosphere in leading up the seasonal development of the stratospheric polar vortex and the subsequent influences on the troposphere. The results confirm previous studies suggesting that the upper stratosphere is not a passive recipient of wave forcing from the troposphere or lower stratosphere (Gray et al. 2003; Albers and Birner 2014; Hitchcock and Haynes 2016). Our results also suggest that improved representation of upper-stratospheric variability in climate models is likely to bring higher fidelity in stratosphere–troposphere coupling. Such improvement could lead to more skillful subseasonal to seasonal prediction both in the stratosphere and the troposphere (see also Gray et al. 2020; Lindgren and Sheshadri 2020). The simplicity of the regime index ζ offers a possibility for it to serve as an additional benchmark for studying stratospheric variability and stratosphere–troposphere coupling. Future work is required to examine whether these results can be reproduced by forecast models such as those employed for extended-range ensemble prediction systems in the Subseasonal to Seasonal Prediction (S2S) Project.

Acknowledgments. This study is part of the British Antarctic Survey (BAS) Polar Science for Planet Earth programme and the National Centre for Atmospheric Science (NCAS) of the Natural Environment Research Council (NERC). HL, LJG, JCK, and TJB also were supported by the NERC North Atlantic Climate System Integrated Study (ACSIS) (NE/N018028). PM was supported by the Japan Society for the Promotion of Science (JSPS) and the Japanese Ministry of Education, Culture, Sports, Science and Technology (MEXT) through the Arctic Challenge for Sustainability (ArCS) Program (JPMXD1300000000). We acknowledge use NCEP CFSR reanalysis data on isentropic coordinates (https://www.ncdc.noaa.gov/data-access/). We thank two anonymous reviewers for constructive comments on earlier versions of the paper.

REFERENCES

Albers, J. R., and T. Birner, 2014: Vortex preconditioning due to planetary and gravity waves prior to sudden stratospheric warmings. *J. Atmos. Sci.*, **71**, 4028–4054, https://doi.org/10.1175/JAS-D-14-0026.1.

Baldwin, M. P., and T. J. Dunkerton, 2001: Stratospheric harbingers of anomalous weather regimes. *Science*, **294**, 581–584, https://doi.org/10.1126/science.1063315.

——, and D. W. J. Thompson, 2009: A critical comparison of stratosphere-troposphere coupling indices. *Quart. J. Roy. Meteor. Soc.*, **135**, 1661–1672, https://doi.org/10.1002/qj.479.

——, D. B. Stephenson, and I. T. Jolliffe, 2009: Spatial weighting and iterative projection methods for EOFs. *J. Climate*, **22**, 234–243, https://doi.org/10.1175/2008JCLI2147.1.

Butler, A. H., D. J. Seidel, S. C. Hardiman, N. Butchart, T. Birner, and A. Match, 2015: Defining sudden stratospheric warmings. *Bull. Amer. Meteor. Soc.*, **96**, 1913–1928, https://doi.org/10.1175/BAMS-D-13-00173.1.

Chang, E. K. M., S. Lee, and K. L. Swanson, 2002: Storm track dynamics. *J. Climate*, **15**, 2163–2183, https://doi.org/10.1175/1520-0442(2002)015<02163:STD>2.0.CO;2.

Charlton-Perez, A. J., L. Ferranti, and R. W. Lee, 2018: The influence of the stratospheric state on North Atlantic weather regimes. *Quart. J. Roy. Meteor. Soc.*, **144**, 1140–1151, https://doi.org/10.1002/qj.3280.

Christiansen, B., 2001: Downward propagation of zonal mean zonal wind anomalies from the stratosphere to the troposphere: Model and reanalysis. *J. Geophys. Res.*, **106**, 27 307–27 322, https://doi.org/10.1029/2000JD000214.

Coughlin, K., and L. J. Gray, 2009: A continuum of sudden stratospheric warmings. *J. Atmos. Sci.*, **66**, 531–540, https://doi.org/10.1175/2008JAS2792.1.

Domeisen, D. I. V., 2019: Estimating the frequency of sudden stratospheric warming events from surface observations of the North Atlantic Oscillation. *J. Geophys. Res. Atmos.*, **124**, 3180–3194, https://doi.org/10.1029/2018JD030077.

——, and Coauthors, 2020: The role of the stratosphere in subseasonal to seasonal prediction: 2. Predictability arising from stratosphere-troposphere coupling. *J. Geophys. Res. Atmos.*, **125,** e2019JD030923, https://doi.org/10.1029/2019JD030923.

Dunkerton, T. J., and D. P. Delisi, 1986: Evolution of potential vorticity in the winter stratosphere of January-February 1979. *J. Geophys. Res.*, **91**, 1199–1208, https://doi.org/10.1029/JD091iD01p01199.

Gerber, E. P., and P. Martineau, 2018: Quantifying the variability of the annular modes: Reanalysis uncertainty vs. sampling uncertainty. *Atmos. Chem. Phys.*, **18**, 17 099–17 117, https://doi.org/10.5194/acp-18-17099-2018.

——, C. Orbe, and L. M. Polvani, 2009: Stratospheric influence on the tropospheric circulation revealed by idealized ensemble forecasts. *Geophys. Res. Lett.*, **36**, L24801, https://doi.org/10.1029/2009GL040913.

Gray, L. J., 2003: The influence of the equatorial upper stratosphere on stratospheric sudden warmings. *Geophys. Res. Lett.*, **30**, 1166, https://doi.org/10.1029/2002GL016430.

——, S. Sparrow, M. Juckes, A. O'Neill, and D. G. Andrews, 2003: Flow regimes in the winter stratosphere of the Northern Hemisphere. *Quart. J. Roy. Meteor. Soc.*, **129**, 925–945, https://doi.org/10.1256/qj.02.82.

——, M. J. Brown, J. Knight, M. Andrews, H. Lu, C. O'Reilly, and J. Anstey, 2020: Forecasting extreme stratospheric polar vortex events. *Nat. Commun.*, **11**, 4630, https://doi.org/10.1038/s41467-020-18299-7.

Greer, K. R., J. P. Thayer, and V. L. Harvey, 2013: A climatology of polar winter stratopause warmings and associated planetary wave breaking. *J. Geophys. Res. Atmos.*, **118**, 4168–4180, https://doi.org/10.1002/jgrd.50289.

——, ——, ——, and E. D. Peck, 2015: Modeling and mechanisms of polar winter upper stratosphere/lower mesosphere disturbances

in WACCM. *J. Geophys. Res. Atmos.*, **120**, 7635–7647, https://doi.org/10.1002/2015JD023471.

Harvey, V. L., and M. H. Hitchman, 1996: A climatology of the Aleutian High. *J. Atmos. Sci.*, **53**, 2088–2102, https://doi.org/10.1175/1520-0469(1996)053<2088:ACOTAH>2.0.CO;2.

——, R. B. Pierce, T. D. Fairlie, and M. H. Hitchman, 2002: A climatology of stratospheric polar vortices and anticyclones. *J. Geophys. Res.*, **107**, 4442, https://doi.org/10.1029/2001JD001471.

Hitchcock, P., and T. G. Shepherd, 2013: Zonal-mean dynamics of extended recoveries from stratospheric sudden warmings. *J. Atmos. Sci.*, **70**, 688–707, https://doi.org/10.1175/JAS-D-12-0111.1.

——, and P. H. Haynes, 2016: Stratospheric control of planetary waves. *Geophys. Res. Lett.*, **43,** 11 884–11 892, https://doi.org/10.1002/2016GL071372.

Hitchman, M. H., and A. S. Huesmann, 2007: A seasonal climatology of Rossby wave breaking in the 320–2000-K layer. *J. Atmos. Sci.*, **64**, 1922–1940, https://doi.org/10.1175/JAS3927.1.

——, and ——, 2009: Seasonal influence of the quasi-biennial oscillation on stratospheric jets and Rossby wave breaking. *J. Atmos. Sci.*, **66**, 935–946, https://doi.org/10.1175/2008JAS2631.1.

Holton, J. R., and H.-C. Tan, 1980: The influence of the equatorial quasi-biennial oscillation on the global circulation at 50 mb. *J. Atmos. Sci.*, **37**, 2200–2208, https://doi.org/10.1175/1520-0469(1980)037<2200:TIOTEQ>2.0.CO;2.

Kidston, J., A. A. Scaife, S. C. Hardiman, D. M. Mitchell, N. Butchart, M. P. Baldwin, and L. J. Gray, 2015: Stratospheric influence on tropospheric jet streams, storm tracks and surface weather. *Nat. Geosci.*, **8**, 433–440, https://doi.org/10.1038/ngeo2424.

Killworth, P. D., and M. E. McIntyre, 1985: Do Rossby-wave critical layers absorb, reflect, or over-reflect? *J. Fluid Mech.*, **161**, 449–492, https://doi.org/10.1017/S0022112085003019.

Kodera, K., and Y. Kuroda, 2002: Dynamical response to the solar cycle. *J. Geophys. Res.*, **107**, 4749, https://doi.org/10.1029/2002JD002224.

——, K. Matthes, K. Shibata, U. Langematz, and Y. Kuroda, 2003: Solar impact on the lower mesospheric subtropical jet: A comparative study with general circulation model simulations. *Geophys. Res. Lett.*, **30**, 1315, https://doi.org/10.1029/2002GL016124.

——, H. Mukougawa, P. Maury, M. Ueda, and C. Claud, 2016: Absorbing and reflecting sudden stratospheric warming events and their relationship with tropospheric circulation. *J. Geophys. Res. Atmos.*, **121**, 80–94, https://doi.org/10.1002/2015JD023359.

Kuroda, Y., and K. Kodera, 2004: Role of the polar-night jet oscillation on the formation of the Arctic Oscillation in the Northern Hemisphere in winter. *J. Geophys. Res.*, **109**, D11112, https://doi.org/10.1029/2003JD004123.

Lindgren, E. A., and A. Sheshadri, 2020: The role of wave–wave interactions in sudden stratospheric warming formation. *Weather Climate Dyn.*, **1**, 93–109, https://doi.org/10.5194/wcd-1-93-2020.

Lu, H., M. P. Baldwin, L. J. Gray, and M. J. Jarvis, 2008: Decadal-scale changes in the effect of the QBO on the northern stratospheric polar vortex. *J. Geophys. Res.*, **113**, D10114, https://doi.org/10.1029/2007JD009647.

——, M. H. Hitchman, L. J. Gray, J. A. Anstey, and S. M. Osprey, 2020: On the role of Rossby wave breaking in the quasi-biennial modulation of the stratospheric polar vortex during boreal winter. *Quart. J. Roy. Meteor. Soc.*, **146**, 1939–1959, https://doi.org/10.1002/qj.3775.

Manney, G. L., R. W. Zurek, A. O'Neill, and R. Swinbank, 1994: On the motion of air through the stratospheric polar vortex. *J. Atmos. Sci.*, **51**, 2973–2994, https://doi.org/10.1175/1520-0469(1994)051<2973:OTMOAT>2.0.CO;2.

——, and Coauthors, 2008: The high Arctic in extreme winters: Vortex, temperature, and MLS and ACE-FTS trace gas evolution. *Atmos. Chem. Phys.*, **8**, 505–522, https://doi.org/10.5194/acp-8-505-2008.

Martineau, P., G. Chen, S.-W. Son, and J. Kim, 2018: Lower-stratospheric control of the frequency of sudden stratospheric warming events. *J. Geophys. Res. Atmos.*, **123**, 3051–3070, https://doi.org/10.1002/2017JD027648.

Matsuno, T., 1971: A dynamical model of the stratospheric sudden warming. *J. Atmos. Sci.*, **28**, 1479–1494, https://doi.org/10.1175/1520-0469(1971)028<1479:ADMOTS>2.0.CO;2.

Maycock, A. C., G. I. T. Masukwedza, P. Hitchcock, and I. R. Simpson, 2020: A regime perspective on the North Atlantic eddy-driven jet response to sudden stratospheric warmings. *J. Climate*, **33**, 3901–3917, https://doi.org/10.1175/JCLI-D-19-0702.1.

McIntyre, M. E., and T. N. Palmer, 1983: Breaking planetary waves in the stratosphere. *Nature*, **305**, 593–600, https://doi.org/10.1038/305593a0.

——, and ——, 1984: The surf zone in the stratosphere. *J. Atmos. Terr. Phys.*, **46**, 825–849, https://doi.org/10.1016/0021-9169(84)90063-1.

Mitchell, D. M., L. J. Gray, J. Anstey, M. P. Baldwin, and A. J. Charlton-Perez, 2013: The influence of stratospheric vortex displacements and splits on surface climate. *J. Climate*, **26**, 2668–2682, https://doi.org/10.1175/JCLI-D-12-00030.1.

O'Neill, A., and V. D. Pope, 1988: Simulations of linear and non-linear disturbances in the stratosphere. *Quart. J. Roy. Meteor. Soc.*, **114**, 1063–1110, https://doi.org/10.1002/qj.49711448210.

——, W. L. Grose, V. D. Pope, H. Maclean, and R. Swinbank, 1994: Evolution of the stratosphere during northern winter 1991/92 as diagnosed from U.K. Meteorological Office analyses. *J. Atmos. Sci.*, **51**, 2800–2817, https://doi.org/10.1175/1520-0469(1994)051<2800:EOTSDN>2.0.CO;2.

Perlwitz, J., and N. Harnik, 2003: Observational evidence of a stratospheric influence on the troposphere by planetary wave reflection. *J. Climate*, **16**, 3011–3026, https://doi.org/10.1175/1520-0442(2003)016<3011:OEOASI>2.0.CO;2.

Polvani, L. M., and R. Saravanan, 2000: The three-dimensional structure of breaking Rossby waves in the polar wintertime stratosphere. *J. Atmos. Sci.*, **57**, 3663–3685, https://doi.org/10.1175/1520-0469(2000)057<3663:TTDSOB>2.0.CO;2.

Saha, S., and Coauthors, 2010: The NCEP Climate Forecast System Reanalysis. *Bull. Amer. Meteor. Soc.*, **91**, 1015–1058, https://doi.org/10.1175/2010BAMS3001.1.

——, and Coauthors, 2014: The NCEP Climate Forecast System version 2. *J. Climate*, **27**, 2185–2208, https://doi.org/10.1175/JCLI-D-12-00823.1.

Scaife, A. A., J. R. Knight, G. K. Vallis, and C. K. Folland, 2005: A stratospheric influence on the winter NAO and North Atlantic surface climate. *Geophys. Res. Lett.*, **32**, L18715, https://doi.org/10.1029/2005GL023226.

——, and Coauthors, 2016: Seasonal winter forecasts and the stratosphere. *Atmos. Sci. Lett.*, **17**, 51–56, https://doi.org/10.1002/asl.598.

Scott, R. K., and L. M. Polvani, 2004: Stratospheric control of upward wave flux near the tropopause. *Geophys. Res. Lett.*, **31**, L02115, https://doi.org/10.1029/2003GL017965.

Sigmond, M., J. F. Scinocca, V. V. Kharin, and T. G. Shepherd, 2013: Enhanced seasonal forecast skill following stratospheric sudden warmings. *Nat. Geosci.*, **6**, 98–102, https://doi.org/10.1038/ngeo1698.

Simpson, I. R., M. Blackburn, and J. D. Haigh, 2009: The role of eddies in driving the tropospheric response to stratospheric heating perturbations. *J. Atmos. Sci.*, **66**, 1347–1365, https://doi.org/10.1175/2008JAS2758.1.

Sivan, Y., S. Rozenberg, A. Halstuch, and A. A. Ishaaya, 2016: Nonlinear wave interactions between short pulses of different spatio-temporal extents. *Sci. Rep.*, **6**, 29010, https://doi.org/10.1038/srep29010.

Thompson, D. W. J., and J. M. Wallace, 1998: The Arctic Oscillation signature in the wintertime geopotential height and temperature fields. *Geophys. Res. Lett.*, **25**, 1297–1300, https://doi.org/10.1029/98GL00950.

——, and ——, 2000: Annular modes in the extratropical circulation. Part I: Month-to-month variability. *J. Climate*, **13**, 1000–1016, https://doi.org/10.1175/1520-0442(2000)013<1000:AMITEC>2.0.CO;2.

Tung, K. K., 1986: Nongeostrophic theory of zonally averaged circulation. Part I: Formulation. *J. Atmos. Sci.*, **43**, 2600–2618, https://doi.org/10.1175/1520-0469(1986)043<2600:NTOZAC>2.0.CO;2.

Waugh, D. W., and D. G. Dritschel, 1999: The dependence of Rossby wave breaking on the vertical structure of the polar vortex. *J. Atmos. Sci.*, **56**, 2359–2375, https://doi.org/10.1175/1520-0469(1999)056<2359:TDORWB>2.0.CO;2.

White, I. P., H. Lu, N. J. Mitchell, and T. Phillips, 2015: Dynamical response to the QBO in the northern winter stratosphere: Signatures in wave forcing and eddy fluxes of potential vorticity. *J. Atmos. Sci.*, **72**, 4487–4507, https://doi.org/10.1175/JAS-D-14-0358.1.

——, C. I. Garfinkel, E. P. Gerber, M. Jucker, V. Aquila, and L. D. Oman, 2018: The downward influence of sudden stratospheric warmings: Association with tropospheric precursors. *J. Climate*, **32**, 85–108, https://doi.org/10.1175/JCLI-D-18-0053.1.